Received: 24 January 2022 | Revised: 18 May 2022 | Accepted: 9 July 2022

DOI: 10.1111/bph.15928

RESEARCH ARTICLE

Ionotropic P2X4 and P2X7 receptors in the regulation of ion transport across rat colon

Jasmin Ballout[1] | Rebecca Claßen[1] | Katrin Richter[2] | Veronika Grau[2] | Martin Diener[1]

[1]Institute for Veterinary Physiology and Biochemistry, Justus Liebig University Giessen, Giessen, Germany

[2]Laboratory of Experimental Surgery, Department of General Surgery, German Centre for Lung Research (DZL), Justus Liebig University Giessen, Giessen, Germany

Correspondence
Martin Diener, Institut für Veterinär-Physiologie und -Biochemie, Justus-Liebig-Universität Gießen, Frankfurter Str. 100, 35392 Giessen, Germany.
Email: martin.diener@vetmed.uni-giessen.de

Background and purpose: ATP plays an important role as an extracellular messenger acting via different types of purinoceptors. Whereas most of the actions of ATP at intestinal epithelia are thought to be mediated by metabotropic P2Y receptors, the role of ionotropic P2X receptors remains unclear. Consequently, we investigated the role of P2X4 and P2X7 receptors on ion transport across rat colonic epithelia by using BzATP, a potent agonist at P2X7 (and weak agonist at P2X4).

Experimental approach: Ussing chamber and Ca^{2+} imaging experiments were performed on rat colonic epithelia, combined with P2X receptor expression studies.

Key results: Ussing chamber experiments revealed that serosal BzATP induced a neuronally mediated increase in short-circuit current caused by Cl^- secretion. In contrast, the effect of mucosal BzATP was smaller, insensitive to tetrodotoxin and Cl^--independent. When epithelia were basolaterally depolarized to measure currents across the apical membrane, BzATP stimulated a cation current consistent with the activation of apical nonselective cation channels. Experiments with isolated colonic crypts revealed a BzATP-induced increase in the cytosolic Ca^{2+} concentration. Sensitivity to antagonists indicates stimulation of P2X4 and P2X7 receptors by serosal BzATP and of P2X7 receptors by mucosal BzATP. A similar pattern was observed with native ATP, which induced larger transepithelial currents in comparison to BzATP. RT-PCR and immunohistochemistry experiments confirmed the expression of P2X4 and P2X7 receptors in the colon localized in the epithelium and in submucosal ganglia.

Conclusions and implications: Epithelial and neuronal ionotropic P2X receptors are involved in the regulation of intestinal ion transport.

KEYWORDS
ATP, epithelium, intestine, ion transport, P2X receptors

Abbreviations: G_t, tissue conductance; I_{sc}, short-circuit current; SERCA, sarcoplasmic/endoplasmic reticulum Ca^{2+} ATPase.

1 | INTRODUCTION

Adenosine 5´-triphosphate (ATP) is not only the key energy source for cellular metabolism, but also plays an important role as an extracellular messenger. Since the seminal work of Burnstock's group, ATP is established as a neurotransmitter released from myenteric neurons to induce intestinal smooth muscle relaxation (Burnstock & Wong, 1978). Signalling by purine analogues has been described as a 'primitive evolutionary system' (Burnstock, 2018), because ATP release is not restricted to purinergic neurons (Burnstock, 2016). Instead, most cells, including immune cells, can release ATP acting as a 'danger signal' during tissue damage or inflammation (Stokes & Surpreanant, 2009). Also in the gut, ATP is released under inflammatory conditions (Brown et al., 2016). If ATP is not set free nonspecifically during cellular damage, controlled release of ATP is mediated predominantly either by exocytosis or by hemichannels in the membrane belonging to the families of **connexin or pannexin proteins** (Dosch et al., 2018). For example, experimental ileitis in rats causes an increase in the ATP release from activated glial cells via **pannexin-1** hemichannels, which—together with changes in ATP degradation—plays an essential role, for example, in modulation of cholinergic neurotransmission and acceleration of the gastrointestinal transit (Vieira et al., 2014, 2017).

Two main classes of membrane receptors mediate the effects of extracellular ATP: metabotropic G protein-coupled **P2Y receptors** and ionotropic **P2X receptors** acting as ligand-gated nonselective cation channels. For P2Y receptors, eight subtypes ($P2Y_{1/2/4/6/11/12/13/14}$) are known, whereas for P2X seven subtypes ($P2X_{1-7}$) have been found, which can be organized as homotrimers or heterotrimers resulting in different functional subunit combinations (Burnstock, 2018).

In the intestinal mucosa, ATP is known to induce a strong anion secretion, which teleologically can be considered as a defence mechanism serving the accelerated expulsion of potentially harmful agents after tissue damage or after stimulation of secretomotor purinergic neurons. Up to now, the effects of ATP at the intestinal epithelium have been exclusively attributed to the stimulation of G protein-coupled P2Y receptors. For example, based on the potency of different purinergic agonists, the actions of ATP at the basolateral (Köttgen et al., 2003; Leipziger et al., 1997) or the apical membrane (Kerstan et al., 1998; Yamamoto & Suzuki, 2002) have been concluded to be mediated by P2Y receptors such as **$P2Y_2$** or **$P2Y_6$**, which are indeed expressed by the intestinal epithelium (Köttgen et al., 2003). In contrast, P2X receptors in the intestine such as, for example, **P2X2** are predominantly considered to modulate the activity of enteric neurons (see, e.g., Ohta et al., 2005), which express, for example, **P2X6** (Yu et al., 2010) or **P2X7** (Palombit et al., 2019; Valdez-Morales et al., 2011).

However, recent data indicate that different epithelia express P2X receptors. Hodges et al. (2009) showed that epithelial cells from rat lacrimal gland express P2X7 and the comparison of potencies of different purinergic agonists suggested the involvement of P2X receptors in the secretory response of bovine oviduct epithelium towards luminal ATP (Keating et al., 2019). In the present study, we asked the question whether stimulation of P2X receptors with the P2X agonist **BzATP**, which stimulates predominantly P2X7 and with a lower potency also **P2X4** receptors (Emmett et al., 2008; Haanes et al., 2012), evokes changes in ion transport across a typical colonic epithelium, such as the rat distal colon, which is able to switch between ion absorption and secretion. This question was addressed by Ussing chamber experiments with mucosal and serosal BzATP (or native ATP) application in the presence or absence of selective P2X receptor blockers and by Ca^{2+} imaging experiments. The colonic mRNA and protein expression of P2X4 and P2X7 was investigated by RT-PCRand immunohistochemistry.

What is already known?

- ATP is both a neurotransmitter as well as a 'danger signal' in the gut.
- Neuronal ionotropic P2X receptors are involved in control of gastrointestinal functions.

What does this study add?

- The colonic epithelium expresses ionotropic P2X4 and P2X7 receptors.
- These receptors are involved in the regulation of epithelial ion transport.

What is the clinical significance?

- Purines released from immune cells are involved in the pathophysiology of inflammatory bowel diseases (IBD).
- Epithelial as well as neuronal P2X receptors may be therapeutic targets for inflammatory conditions.

2 | METHODS

2.1 | Animals

All animal care and experimental procedures were approved by the named animal welfare officers of the Justus Liebig University (administrative number 577_M) and performed according to the German and European animal welfare law. Animal studies are reported in compliance with the ARRIVE guidelines (Percie du Sert et al., 2020) and with the recommendations made by the *British Journal of Pharmacology* (Lilley et al., 2020). Male and female Wistar rats (RRID:RGD_13508588) with an age between 6 and 8 weeks (about 200- to 300-g

body mass) were used. The animals were bred and housed at the Institute of Veterinary Physiology and Biochemistry of the Justus Liebig University under specified pathogen free conditions. They had free access to a standard rat diet (*ssniff® R-Z*; Sniff, Soest, Germany) and water. Animals were housed in macrolone type IV cages using standard bedding material (LT E-001; Abedd, Vienna, Austria) with two to three animals per cage at 22°C, 50% air humidity and a light–dark cycle of 12:12 h. Animals were killed after CO_2 narcosis by cervical dislocation followed by exsanguination.

2.2 | Solutions

Ussing chamber experiments were carried out in Parsons solution of the following composition (in mmol·L^{-1}): 107 NaCl, 4.5 KCl, 25 $NaHCO_3$, 1.8 Na_2HPO_4, 0.2 NaH_2PO_4, 1.25 $CaCl_2$, 1 $MgSO_4$, 12.2 glucose. The solution was gassed with 5% (v/v) CO_2 and 95% (v/v) O_2 at 37°C and had a pH of 7.4 (adjusted by 1 N NaOH/HCl). For basolateral depolarization, NaCl was equimolarly replaced by KCl (111.5-mmol·L^{-1} KCl buffer) in the serosal buffer. When Na^+ currents across the apical membrane had to be eliminated during basolateral depolarization experiments, NaCl in the mucosal buffer was equimolarly substituted by NMDG (N-methyl-D-glucamine) Cl (107-mmol·L^{-1} NMDG Cl/4.5-mmol·L^{-1} KCl buffer).

For crypt isolation, Ca^{2+}- and Mg^{2+}-free Hanks balanced salt solution (HBSS; Thermo Fisher Scientific, Darmstadt, Germany) containing 10-mmol·L^{-1} ethylenediaminotetraacetic acid (EDTA) was used. The pH was adjusted to 7.4 by tris (hydroxymethyl)-aminomethane. The isolated crypts were stored in a high potassium Tyrode's solution consisting of (in mmol·L^{-1}): 100 K gluconate, 30 KCl, 20 NaCl, 1.25 $CaCl_2$, 1 $MgCl_2$, 10 HEPES (N-[2-hydroxyethyl] piperazine-N′-2-ethanesulfonic acid), 12.2 glucose, 5 Na pyruvate and 1-g·L^{-1} bovine serum albumin (BSA); pH was set to 7.4 (adjusted by KOH). Imaging experiments were performed in Tyrode's solution containing (in mmol·L^{-1}) 140 NaC1, 5.4 KC1, 1.25 $CaC1_2$, 1 $MgCl_2$, 12.2 glucose, 10 HEPES, 5 Na pyruvate and 1-g·L^{-1} BSA, adjusted to pH of 7.4 with NaOH/HCl.

All immunohistochemical stainings were performed with phosphate buffer (PB), consisting of 80-mmol·L^{-1} Na_2HPO_4 and 20-mmol·L^{-1} NaH_2PO_4 with pH of 7.4 (adjusted by 1 N NaOH/HCl).

2.3 | Tissue preparation

The distal colon, which is a well-established model to study epithelial anion secretion, was dissected and its lumen was flushed several times with ice cold Parsons solution before it was mounted on a thin plastic rod. A circular incision was made with a scalpel near the distal end. The serosa and the tunica muscularis were stripped off manually in order to obtain mucosa-submucosa preparations. Two segments of the distal colon of each rat were used for Ussing chamber experiments. One segment was treated with putative inhibitors; the other segment was only treated with the solvent of the respective inhibitor. Segments were randomly distributed by a technician and calculation of drug effects were performed by programmed scripts in Excel^R, so that no blinding was necessary for these experiments.

For isolation of intact crypts, the mucosa-submucosa preparations of distal colon were mounted on a holder with tissue adhesive (cyanoacrylate) and incubated for approximately 8 min in EDTA-containing HBSS at 37°C gassed with ambient air. After incubation, the holder was fixed on a vibrating machine (Chemap, Volketswil, Switzerland) and vibrated once for about 30 s in order to release crypts. Isolated crypts were collected and stored in a high K^+ Tyrode's buffer with a low Cl^- content (Del Castillo, 1987) before they were attached to poly-L-lysine (0.1 mg·ml^{-1}; Cell Systems, Troisdorf, Germany) coated cover slips with a diameter of 22 mm for imaging experiments. For fixation of the tissue for immunohistochemical experiments, whole-mount segments from rat distal colon were rinsed with ice cold Parsons solution, opened longitudinally and mounted on a holder with tissue adhesive (cyanoacrylate).

2.4 | Ussing chamber experiments

The mucosa-submucosa preparations were mounted in a modified Ussing chamber, bathed with a volume of 3.5 ml on each side and gassed with carbogen (5% CO_2, 95% O_2, v/v). The tissue was incubated at 37°C and short-circuited by a computer-controlled voltage-clamp device (Ingenieur Büro für Mess- und Datentechnik Mussler, Aachen, Germany) with correction for solution resistance. The exposed surface of the tissue was 1 cm^2. The electrodes used for voltage measurement and current application were Ag/AgCl electrodes in 3 mol·L^{-1} KCl, which were separated from the chamber lumen by agar bridges (46.7 g·L^{-1} agar in the standard bathing solution). Short-circuit current (I_{sc}) was continuously recorded, and tissue conductance (G_t) was measured every minute by applying a current pulse of ±50 μA·cm^{-2} with a duration of 200 ms. I_{sc} is expressed as μEq·h^{-1}·cm^{-2}, that is, the flux of a monovalent ion per time and area with 1 μEq·h^{-1}·cm^{-2} = 26.9 μA·cm^{-2}. An increase of I_{sc} reflects an enhanced anion secretion or cation absorption, respectively. Drugs were administered after an equilibration period of about 60 min. The maximal increase in I_{sc} evoked by an agonist is given as the difference to the baseline value just prior administration of the drug (ΔI_{sc}). In order to quantify the effects of putative inhibitors on baseline I_{sc} (Table S1), the I_{sc} was averaged during a 3-min interval starting 5 min after administration of the putative inhibitor and expressed as the difference to the baseline value just prior administration of the drug (ΔI_{sc}).

2.5 | Imaging experiments with fura-2

Isolated crypts were attached to poly-L-lysine coated cover slips and loaded for at least 120 min with 6-μmol·L^{-1} fura-2 acetoxymethylesther (fura-2/AM, Thermo Fisher Scientific) mixed with an equal volume of pluronic F-127 (20% [w/v] stock solution in DMSO; Thermo Fisher Scientific) at room temperature. After the loading period, the

dye not taken up by the cells was washed away. The cover slip was transferred into an imaging chamber with a volume of 2 ml, and the experiments were carried out in Tyrode's solution at room temperature.

The imaging experiments were performed with an inverted microscope (Olympus IX-50; Olympus, Hamburg, Germany), equipped with an epifluorescence set-up and an image analysis system (Till Photonics, Martinsried, Germany). The isolated crypts were excited with 340 and 380 nm and emission was measured at wavelength >440 nm. The fura-2 ratio (emission at the excitation wavelength of 340 nm per emission at the excitation wave length of 380 nm) was used to monitor changes in cytosolic Ca^{2+} concentration. Several regions of interest (ROI), each with the size of about one individual cell, were selected in each crypt. Data were sampled at 0.2 Hz. The baseline of the fluorescence signal was measured for several minutes before any drug was added. A response to a purinergic agonist was accepted by definition when two conditions were fulfilled simultaneously:

1. The amplitude of the change exceeded the 4-fold standard deviation of the scattering in the fura-2 ratio during the control period just prior to addition of the drug.
2. The amplitude of the change in the fura-2 ratio exceeded an absolute value of 0.1.

At the end of each experiment, **cyclopiazonic acid** (CPA, $5{\cdot}10^{-6}$ mol·L^{-1}), a blocker of sarcoplasmic/endoplasmic reticulum Ca^{2+}-ATPase (SERCA), was administered as a viability control. Cells were accepted as viable if either a purinergic agonist or CPA induced an increase in the fura-2 ratio.

2.6 | RT-PCR experiments

For RT-PCR studies, samples from whole colonic wall, colonic mucosal scrapings, kidney, spinal cord, dorsal root ganglia or liver were transferred into lysis buffer (Macherey-Nagel, Düren, Germany) and homogenized using a mixer mill (NM301; Retsch, Haan, Germany) with a frequency of 30 Hz for about 2 min. Total RNA was extracted using the Nucleo Spin® RNA Plus kit (Macherey-Nagel). RNA was transcribed into cDNA with Tetro cDNA synthesis Kit (Bioline, Luckenwalde, Germany).

For the PCR reaction, Bioline®Mangomix (Bioline, Germany) was used with 5 mmol·L^{-1} $MgCl_2$. Primers (for sequences and references, see Table 1) were obtained from Eurofins MWG Synthesis, Ebersberg, Germany. Each PCR started with a denaturation period of 0.5 min at 95°C, followed by an annealing phase of 0.5 min at 58°C and an elongation phase of 1 min at 72°C; the whole cycle was repeated 35 times. For control of the PCR reaction glyceraldehyde-3-phosphate dehydrogenase (GAPDH) was used; negative controls were performed with RNA/DNA-free water. The reaction product was visualized after electrophoresis in a 3% (w/v) high-resolution agarose gel (Carl Roth, Karlsruhe, Germany) and staining with Roti®-Gel Stain (Carl Roth). At least three different biological replicates and two technical replicates

TABLE 1 Primers

Target	Gene number	Forward	Backward	Expected product size	Reference
P2X1	NM_012997.3	5′-CAGCTTTCCACGCTTCAAGG-3′	5′-CAACCACCCCACCCTTCTCA-3′	182 bp	Haanes and Edvinsson (2014)
P2X2	NM_053656.3	5′-CGACGACTGTATTGCCG-3′	5′-CTCCAATGACACCGCC-3′	374 bp	Li et al. (2020)
P2X3	NM_031075.2	5′-TGGCGTTCTGGGTATTAAGATCGG-3′	5′-CAGTGGCCTGGTCACTGGCGA-3′	440 bp	Li et al. (2020)
P2X4	NM_031594.2	5′-GAGGCATCATGGGTATCCAGATCAAG-3′	5′-GAGCGGGGTGGAAATGTAACTTTAG-3′	447 bp	Li et al. (2020)
P2X5	NM_080780.3	5′-CGACTGGGGTCTATTGTCG-3′	5′-CCTGGCGAACCTGAAGTTGT-3′	201 bp	Haanes and Edvinsson (2014)
P2X6	X97376.1	5′-AAAGACTGGTCAGTGTGTGGGTTC-3′	5′-TGCCTGCCCAGTGACAAGAATGTCAA-3′	520 bp	Li et al. (2020)
P2X7	NM_019256.2	5′-GTGCCATTCTGACCAGGGTTGTATAAA-3′	5′-GCCACCTCTGTAAAGTTCTCTCCGATT-3′	354 bp	Li et al. (2020)
P2X7(a)	FJ436445.1	5′-ACATGACCGTCTTTTCCTAC-3	5′-ACCTGGTAAGATGTTTCTCG-3′	551 bp	Nicke et al. (2009)
P2X7(k)	FJ436445.1	5′-GCCAGTGAGACATTTATGC-3′	5′-ACCTGGTAAGATGTTTCTCG-3′	619 bp	Nicke et al. (2009)
GAPDH	BC059110	5′-ACGGGAAGCTCACTGGCATG-3′	5′-CCACCACCCTGTTGCTGTAG-3′	303 bp	Pouokam et al. (2013)

Note: Gene numbers refer to http://www.ncbi.nlm.nih.gov.

were performed for each target gene in the RT-PCR. The PCR products were manually excised from the gel and isolated using the MinElute Gel Extraction Kit (QIAGEN, Hilden, Germany) according to the manufacturer's instructions. Purified products were sequenced by a custom sequencing service (Eurofins MWG Operon, Ebersberg, Germany).

2.7 | Immunohistochemistry

Details of immunohistochemical protocols are described in the following, according to *BJP* guidelines (Alexander et al., 2018). Segments of rat distal colon were fixed in phosphate buffer (PB) containing 4% (w/v) paraformaldehyde at 4°C overnight, rinsed three times in PB for 1 h, embedded in gelatine (100 $g \cdot L^{-1}$) and frozen in N_2-cooled isopentane. The 4-μm thick sections were mounted on microscope slides (Superfrost® Plus, Thermo Fisher Scientific). After three washing steps with PB for 5 min each, sections were incubated for 2 h in a blocking solution containing PB with 0.2% (v/v) Triton-X-100, 3% (w/v) BSA and 10% (v/v) donkey serum. The primary antibodies were dissolved in PB containing 0.1% (v/v) Triton-X-100, 1% (w/v) BSA, 0.5% (w/v) milk powder and 1% (v/v) donkey serum. The sections were incubated with the primary antibodies overnight at 4°C. Primary antibodies were anti-P2X4 (rabbit polyclonal IgG; Alomone Labs, Jerusalem, Israel, #APR-002, RRID:AB_2040058; dilution 1:200), anti-P2X7 (rabbit polyclonal IgG; Alomone Labs, Jerusalem, Israel, #APR-004, RRID:AB_2040068; dilution 1:200) and anti-MAP 2 (mouse antibody against microtubule associating protein-2; Sigma, #M1406, RRID:AB_477171; dilution 1:250). Both antibodies used for P2X detection have been validated in knock-out mice (Apolloni et al., 2013; Sim et al., 2006). After threefold washing with PB for 5 min, sections were loaded with secondary antibodies for 1 h at room temperature. Primary antibodies for P2X4 and P2X7 were combined with Cy3 donkey anti-rabbit immunoglobulins (Dianova, Hamburg, Germany, #711-165-152, RRID:AB_2307443; dilution 1:1000), whereas MAP 2 was combined with Alexa488 goat anti-mouse immunoglobulins (Thermo Fisher, #A-11029, RRID:AB_2534088; dilution 1:500). RotiFluo with **DAPI** (4,6-diamidio-2-phenylindoldilactate, Roth, Karlsruhe, Germany) was used for nucleus staining and coverslipping. Pictures were taken with the fluorescence microscope Nikon 80i (Nikon, Düsseldorf, Germany).

2.8 | Materials

Tetrodotoxin (CAS 4368-28-9) was dissolved in $2 \cdot 10^{-2}$-$mol \cdot L^{-1}$ citrate buffer. **Bumetanide** (CAS 28395-03-1) and **forskolin** (CAS 66575-29-9; Tocris) were dissolved in ethanol (final ethanol concentration 0.3 $ml \cdot L^{-1}$). **A438079** (3-(5-[2,3-dichlorophenyl]-1H-tetrazol-1-yl)methyl pyridine hydrochloride; CAS 899507–36-9; Tocris), **AZ10606120** (N-[2-[[2-[[2-ydroxyethyl]amino]ethyl]amino]-5-quinolinyl]-2-tricyclo[3.3.1.13,7]dec-1-ylacetamide dihydrochloride; CAS 607378-18-7; Tocris), **5-BDBD** (5-[3-bromophenyl]-1,3-dihydro-2H-benzofuro[3,2-e]-1,4-diazepin-2-one; CAS 768404–03-1; Tocris), cyclopiazonic acid (CAS 18172–33-3) and **ivermectin** (22,23-dihydroavermectin B1; CAS 70288–86-7; Tocris) were dissolved in DMSO (final maximal DMSO concentration 4 $ml \cdot L^{-1}$). **ARL 67156** (6-N,N-diethyl-D-ß,γ-dibromomethyleneATP trisodium salt; CAS 1021868–83-6; Tocris), ATP (adenosine 5′-triphosphate disodium salt; CAS 987–65-5), **atropine** sulphate (CAS: 5908-99-6), $BaCl_2$, BzATP (2′/3′-O-(4-benzoylbenzoyl)adenosine-5′-triphosphate (triethylammonium) salt; CAS 112898-15-4; Jena Bioscience, Jena, Germany), **carbachol** (CAS 51-83-2) and **hexamethonium** chloride (CAS 60-25-3) were dissolved in distilled water. If not indicated differently, salts/reagents were obtained from Sigma.

2.9 | Data and statistical analysis

The data and statistical analysis comply with the recommendations on experimental design and analysis in pharmacology (Curtis et al., 2018). Results are given as mean ± SEM with the number (n) of investigated tissues. For all Ussing chamber experiments, a group size of $n = 6–8$ was designed. In imaging experiments, n refers to the number of measured cells in isolated crypts, which were prepared from at least three different individual animals for each experimental series. For the comparison of two groups, either Student's *t* test (paired or unpaired as appropriate) or Mann–Whitney *U*-test was applied. An *F*-test decided which test method had to be used. Fittings of the I_{sc} data to non-linear functions were performed with GraphPad Prism 7.02 (GraphPad Software, La Jolla, CA, USA). Statistical analysis was only performed when group size was at least $n = 5$ independent biological samples.

2.10 | Nomenclature of targets and ligands

Key protein targets and ligands in this article are hyperlinked to corresponding entries in http://www.guidetopharmacology.org, the common portal for data from the IUPHAR/BPS Guide to PHARMACOLOGY (Harding et al., 2018), and are permanently archived in the Concise Guide to PHARMACOLOGY 2021/22 (Alexander et al., 2021).

3 | RESULTS

3.1 | Side-dependent effect of BzATP in rat colonic mucosa-submucosa preparations

The $P2X_7$ agonist, BzATP (10^{-7}–10^{-4} $mol \cdot L^{-1}$), induced a concentration-dependent increase in I_{sc} across rat colonic mucosa-submucosa preparations (Figure 1). When administered at the serosal side, the agonist induced a transient peak in I_{sc}, which decayed with a time constant of 6.6 min (measured for a concentration of 10^{-4} $mol \cdot L^{-1}$) when the data were fitted to a monoexponential decay function (Figure 2a). In contrast, when administered to the mucosal side, the increase in I_{sc} developed more slowly within 10–15 min and also the maximal increase was smaller compared to that induced by

serosal administration of the agonist (Figure 2b). The increase in I_{sc} was paralleled by a modest increase in tissue conductance (G_t; Figure 2c,d), especially after mucosal administration. This increase was completely reversible upon washout of the drug (Figure 2c,d),

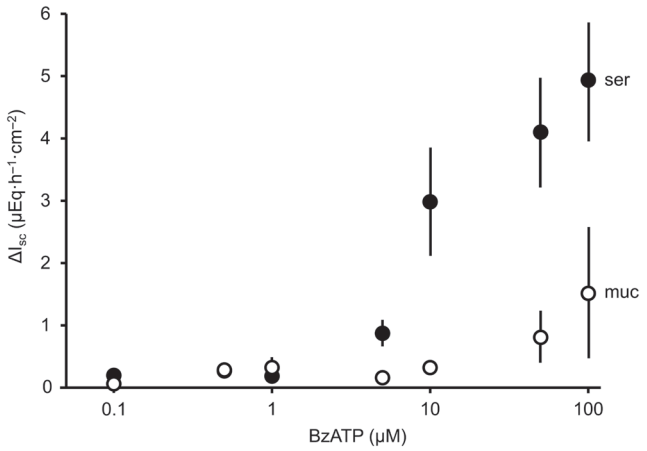

FIGURE 1 Concentration-dependent effect of serosal (closed circles) or mucosal (open circles) BzATP on short-circuit current (I_{sc}) across mucosa-submucosa preparations from rat distal colon. The curves were constructed from two independent experimental series, in which concentrations from 10^{-7}–$5 \cdot 10^{-6}$ or 10^{-5}–10^{-4} mol·L^{-1} were administered, respectively. Values are means (symbols) ± SEM (lines; partially covered by the symbols); n = 5 for concentrations ≥10^{-5} mol·L^{-1} and n = 6 for concentrations <10^{-5} mol·L^{-1} (both for mucosal and serosal administration).

excluding damage of the epithelium by the formation of large pores which has been reported to occur after prolonged exposure of cells to BzATP (see, e.g., Virginio et al., 1997).

Different ionic mechanisms underlie these two current responses. The effect of serosally administered BzATP ($5 \cdot 10^{-5}$ mol·L^{-1}) was reduced by 85% ($P < 0.05$), when Cl^- was replaced on both sides of the tissue by the impermeant anion, gluconate (Table 2). A significant inhibition (by about 65%; $P < 0.05$) of the I_{sc} response also was observed when tissues had been pretreated with bumetanide (10^{-4} mol·L^{-1} at the serosal side), a potent inhibitor of the Na^+-K^+-$2Cl^-$-cotransporter (NKCC) in the basolateral membrane, which is the predominant transporter for Cl^- uptake in secretory epithelia. As expected, the increase in I_{sc} evoked by the viability controls at the end of the experiments, that is, the Ca^{2+}-dependent secretagogue, carbachol ($5 \cdot 10^{-5}$ mol·L^{-1} at the serosal side) and the cAMP-dependent secretagogue, forskolin ($9 \cdot 10^{-6}$ mol·L^{-1} at the mucosal and serosal sides), also was inhibited by gluconate and butmetanide, although the reduction of the forskolin-stimulated current did not reach statistical significance in case of bumetanide (Table 2). Consequently, the I_{sc} induced by serosal BzATP is carried by Cl^- secretion. In contrast, neither substitution of Cl^- by an impermeant gluconate nor by bumetanide had a significant effect on the current evoked by mucosally administered BzATP ($5 \cdot 10^{-5}$ mol·L^{-1} at the mucosal side; Table 3).

Chloride secretion across anion channels needs a negative membrane potential (generated by a K^+ diffusion potential) as driving force for cellular extrusion of Cl^- via anion channels. Thus, we investigated whether the current induced by BzATP was inhibited by Ba^{2+}, a broad

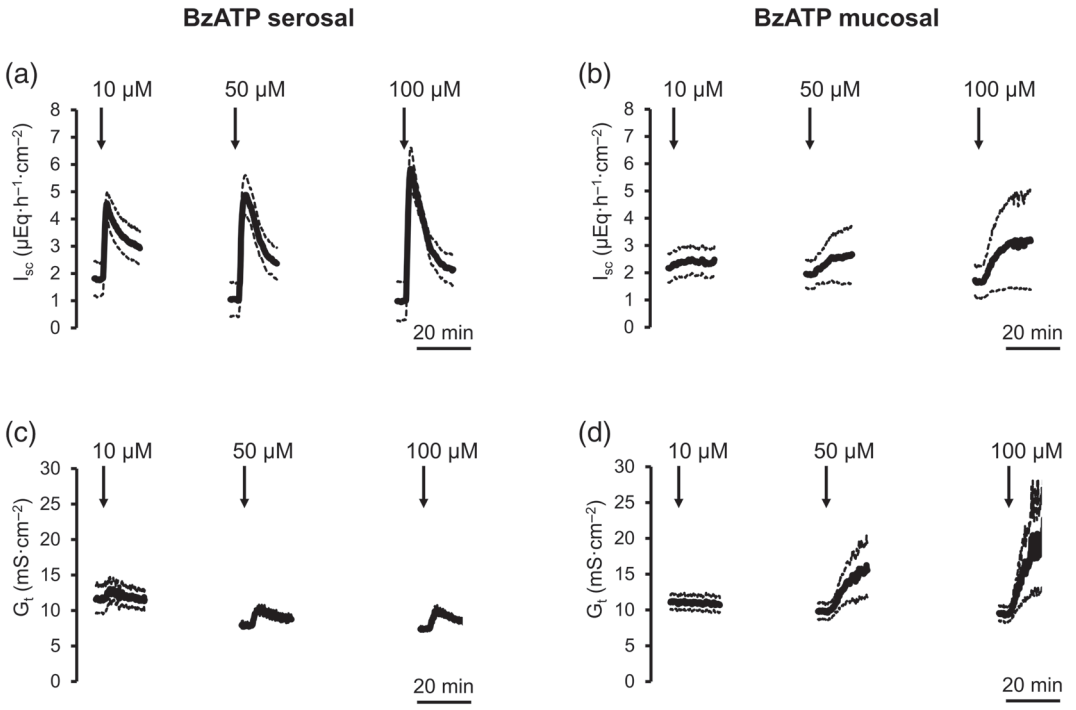

FIGURE 2 Time course of the effect of serosal (a, c) or mucosal (b, d) BzATP on short-circuit current (I_{sc}; a, b) or tissue conductance (G_t; c, d) across mucosa–submucosa preparations from rat distal colon. Line interruptions are caused by omission of washing phases. Values are means (solid lines) ± SEM (dotted lines); n = 5 for both experimental series.

TABLE 2 Effect of BzATP administered to the serosal side of distal colon

	Change in BzATP response	BzATP ($5{\cdot}10^{-5}$ mol·L^{-1})	Carbachol ($5{\cdot}10^{-5}$ mol·L^{-1})	Forskolin ($9{\cdot}10^{-6}$ mol·L^{-1})	n
			ΔI_{sc} (μEq·h^{-1}·cm^{-2})		
Mucosal + serosal side					
+ Cl^-		5.18 ± 1.04	11.63 ± 1.02	4.12 ± 0.81	6
− Cl^-	↓	0.78 ± 0.45*	1.65 ± 0.60*	0.98 ± 0.33*	6
Mucosal side					
− Ba^{2+}		2.81 ± 0.64	10.86 ± 1.55	2.12 ± 0.25	8
+ Ba^{2+} (10^{-2} mol·L^{-1})		1.55 ± 0.47	10.95 ± 1.06	1.71 ± 0.25	7
Serosal side					
− Bumetanide		3.29 ± 0.47	9.63 ± 1.07	2.92 ± 0.79	8
+ Bumetanide (10^{-4} mol·L^{-1})	↓	1.15 ± 0.31*	1.68 ± 0.32*	0.96 ± 0.23	7
− Tetrodotoxin		4.59 ± 1.17	8.94 ± 1.09	2.14 ± 0.52	5
+ Tetrodotoxin (10^{-6} mol·L^{-1})	↓	0.57 ± 0.08*	7.29 ± 1.26	2.55 ± 0.55	6
− Atropine		3.77 ± 0.63	8.57 ± 1.23	3.31 ± 0.89	7
+ Atropine (10^{-5} mol·L^{-1})		4.23 ± 1.03	2.32 ± 0.62*	5.27 ± 1.23	7
− Hexamethonium		3.73 ± 0.57	9.88 ± 0.83	3.22 ± 0.26	6
+ Hexamethonium (10^{-4} mol·L^{-1})		3.66 ± 0.84	10.22 ± 1.70	2.53 ± 0.60	6
− Ba^{2+}		3.40 ± 0.65	9.14 ± 1.06	1.57 ± 0.11	8
+ Ba^{2+} (10^{-2} mol·L^{-1})	↓	0.12 ± 0.07*	9.00 ± 0.63	0.11 ± 0.07	8
− A438079		3.01 ± 0.56	12.77 ± 1.15	1.32 ± 0.32	6
+ A438079 (10^{-4} mol·L^{-1})		3.35 ± 0.97	10.72 ± 1.13	0.27 ± 0.16*	6
− AZ10606120		2.54 ± 0.92	11.31 ± 1.10	1.24 ± 0.27	6
+ AZ10606120 ($5{\cdot}10^{-5}$ mol·L^{-1})	↓	0.27 ± 0.12*	9.84 ± 1.47	1.19 ± 0.35	6
− 5-BDBD		4.23 ± 1.00	12.67 ± 1.03	2.02 ± 0.18	8
+ 5-BDBD (10^{-5} mol·L^{-1})	↓	1.24 ± 0.37*	10.94 ± 1.58	1.02 ± 0.24	8

Note: Increase in I_{sc} induced by BzATP (at the serosal side), carbachol (at the serosal side) and forskolin (at the mucosal and serosal side) in rat distal colon. Responses were tested in the presence and absence of different drugs administered on either the mucosal or serosal side, or both. A438079 and AZ10606120 are used as P2X7 antagonists, 5-BDBD as P2X4 antagonist. Effects of drugs or anion replacement on baseline I_{sc} are shown in Table S1 (pooled data from all experiments depicted in Tables 2–5 with the same inhibitor). Values are given as change in I_{sc} versus baseline just prior administration of the individual secretagogue (ΔI_{sc}) and are means ± SEM.

*$P < 0.05$ versus response of the same secretagogue in the corresponding control series.

blocker of many types of K^+ channels. As expected, the I_{sc} induced by serosal BzATP ($5{\cdot}10^{-5}$ mol·L^{-1}) was inhibited by 95% ($n = 8$, $P < 0.05$) in the presence of serosal Ba^{2+} (10^{-2} mol·L^{-1}), whereas mucosal Ba^{2+} in the same concentration was ineffective (Table 2). Interestingly, in the case of mucosally administered BzATP ($5{\cdot}10^{-5}$ mol·L^{-1}), serosal Ba^{2+} inhibited the I_{sc} induced by the purinergic agonist by about 75% and mucosal Ba^{2+} even reverted the I_{sc} induced by BzATP into a negative current (Table 3). This paradox negative current cannot be explained by blockade of apical K^+ channels, because electrogenic K^+ secretion itself would lead to a negative I_{sc}, so indicating that other mechanisms must be involved (see Section 4).

3.2 | Involvement of secretomotor neurons

In case of serosal BzATP ($5{\cdot}10^{-5}$ mol·L^{-1}), the secretory response was inhibited by about 85% ($P < 0.05$, Table 2) when tissues were pretreated with tetrodotoxin (10^{-6} mol·L^{-1} at the serosal side), a blocker of neuronal voltage-dependent Na^+ channels (Catterall, 1980) indicating the activation of submucosal secretomotor neurons by the purinergic agonist. Obviously, cholinergic neurons, which play a prominent part in the neuronal regulation of epithelial ion transport (Diener et al., 1989), were not involved, because neither the muscarinic antagonist, atropine (10^{-5} mol·L^{-1} at the serosal side), nor the nicotinic antagonist, hexamethonium (10^{-4} mol·L^{-1} at the serosal side), inhibited the current induced by serosal BzATP (Table 2).

Well-known excitatory purinergic receptors on enteric neurons are **$P2Y_1$ receptors** (Hu et al., 2003). Consequently, we tested whether the tetrodotoxin-sensitive component of the response to serosal BzATP was preserved after pretreatment with the $P2Y_1$ blocker **MRS2500**. BzATP ($5{\cdot}10^{-5}$ mol·L^{-1} at the serosal side) evoked an increase in I_{sc} in the presence of MRS2500 (1 μmol·L^{-1} at the serosal side), which amounted to 0.90 ± 0.36 μEq·h^{-1}·cm^{-2} ($n = 6$). This

TABLE 3 Effect of BzATP administered to the mucosal side of distal colon

	Change in BzATP response	BzATP ($5{\cdot}10^{-5}$ mol·L^{-1})	Carbachol ($5{\cdot}10^{-5}$ mol·L^{-1})	Forskolin ($9{\cdot}10^{-6}$ mol·L^{-1})	n
		ΔI_{sc} (μEq·h^{-1}·cm^{-2})			
Mucosal + serosal side					
+ Cl^-		0.33 ± 0.11	9.77 ± 1.54	3.12 ± 0.71	6
− Cl^-		0.29 ± 0.16	1.72 ± 0.33*	1.33 ± 0.21*	6
Mucosal side					
− Ba^{2+}		0.19 ± 0.06	14.32 ± 1.27	2.71 ± 0.36	7
+ Ba^{2+} (10^{-2} mol·L^{-1})	↓	−0.03 ± 0.04*	10.43 ± 0.98*	1.46 ± 0.19*	8
− A438079		0.20 ± 0.15	15.47 ± 2.18	1.81 ± 0.29	6
+ A438079 (10^{-4} mol·L^{-1})		0.11 ± 0.10	14.28 ± 1.63	1.03 ± 0.23	6
− AZ10606120		0.29 ± 0.11	11.97 ± 1.59	2.37 ± 0.46	7
+ AZ10606120 ($5{\cdot}10^{-5}$ mol·L^{-1})	↓	0.01 ± 0.01*	12.61 ± 0.78	2.57 ± 0.34	7
− 5-BDBD		0.30 ± 0.13	11.89 ± 1.47	3.32 ± 1.26	8
+ 5-BDBD (10^{-5} mol·L^{-1})		0.13 ± 0.06	14.36 ± 1.13	0.79 ± 0.31	8
Serosal side					
− Bumetanide		0.37 ± 0.09	13.34 ± 2.10	2.06 ± 0.49	7
+ Bumetanide (10^{-4} mol·L^{-1})		0.60 ± 0.25	2.30 ± 0.29*	1.40 ± 0.29	7
− Tetrodotoxin		0.75 ± 0.24	7.41 ± 1.25	2.00 ± 0.45	6
+ Tetrodotoxin (10^{-6} mol·L^{-1})		0.43 ± 0.12	8.42 ± 0.91	3.73 ± 0.38*	6
− Ba^{2+}		0.89 ± 0.43	11.63 ± 2.29	1.60 ± 0.31	6
+ Ba^{2+} (10^{-2} mol·L^{-1})	↓	0.20 ± 0.07*	8.88 ± 1.11	0.33 ± 0.09*	6

Note: Increase in I_{sc} induced by BzATP (at the mucosal side), carbachol (at the serosal side) and forskolin (at the mucosal and serosal side) in rat distal colon. Responses were tested in the presence and absence of different drugs administered on either the mucosal or serosal side or both. A438079 and AZ10606120 are used as P2X7 antagonists, 5-BDBD as P2X4 antagonist. Effects of drugs or anion replacement on baseline I_{sc} are shown in Table S1 (pooled data from all experiments depicted in Tables 2–5 with the same inhibitor). Values are given as change in I_{sc} versus baseline just prior administration of the individual secretagogue (ΔI_{sc}) and are means ± SEM.

*$P < 0.05$ versus response of the same secretagogue in the corresponding control series.

response was reduced significantly to 0.17 ± 0.07 μEq·h^{-1}·cm^{-2} (n = 6), when the tissues were pretreated with tetrodotoxin (1 μmol·L^{-1} at the serosal side) in addition. This suggests that a stimulation of neuronal $P2Y_1$ receptors is not responsible for the effect of BzATP.

Moreover, the I_{sc} induced by mucosal BzATP ($5{\cdot}10^{-5}$ mol·L^{-1}) was not significantly inhibited by tetrodotoxin, indicating a direct effect on the epithelium (Table 3).

3.3 | Apical cation currents activated by BzATP

Resistance against bumetanide and the observation that replacement of Cl^- by gluconate did not affect the I_{sc} induced by mucosal BzATP indicated that anion secretion does not underlie the BzATP-induced I_{sc}. In order to find out whether this current might directly reflect the cation flow across activated P2X receptors, which work as nonselective cation channels (for review, see Burnstock, 2018), currents across the apical membrane were measured after mucosal application of BzATP. The basolateral membrane potential was 'electrically eliminated' by depolarization with a buffer containing a high K^+ concentration. Due to the high basolateral K^+ conductance, the electrical properties of the tissue, which are normally characterized by two batteries in series, are then dominated by the apical membrane (Fuchs et al., 1977; Schultheiss & Diener, 1997). Serosal administration of a high K^+ buffer led to a large negative I_{sc}, which has to be expected from the resulting diffusion potential (Figure 3a). When BzATP was administered to the basolaterally depolarized epithelia in the presence of mucosal Na^+, a large positive I_{sc} was induced (Figure 3a). On average, BzATP (10^{-4} mol·L^{-1} at the mucosal side) induced a sustained positive I_{sc}, which would be in accordance with a flow of Na^+ into the epithelial cells, amounting 1.94 ± 0.31 μEq·h^{-1}·cm^{-2} (n = 8; $P < 0.05$ vs. time-dependent control), whereas in time-dependent control experiments (n = 8) I_{sc} remained stable during the basolateral depolarization. In order to prove that the BzATP-induced positive I_{sc} across the apical membrane was carried by Na^+, cation replacement experiments where performed in which Na^+ in the mucosal compartment was substituted by the impermeant cation, $NMDG^+$. Under these conditions, BzATP (10^{-4} mol·L^{-1} at the mucosal side) could not induce a stable increase in I_{sc} anymore but led to a transient stimulation of a negative I_{sc} (Figure 3b). This would be consistent with the transient activation of an apical K^+ conductance.

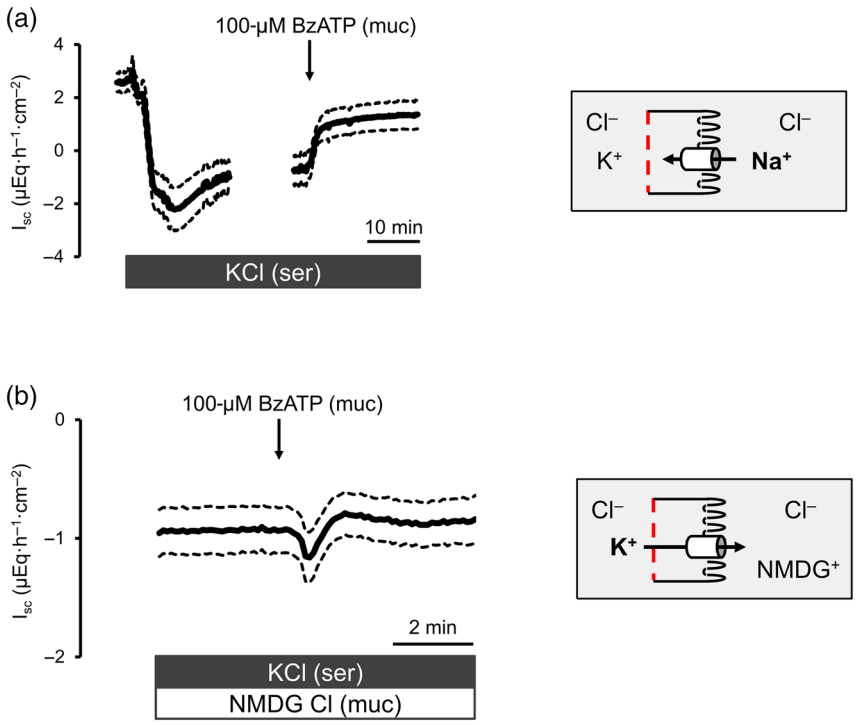

FIGURE 3 Effect of BzATP (10^{-4} mol·L^{-1} at the mucosal side) on currents across the apical membrane after basolateral depolarization (serosal solution: 111.5-mmol·L^{-1} KCl). (a) BzATP-induced currents across a Na^+-permeable, presumably nonselective cation conductance were measured in the presence of 107-mmol·L^{-1} NaCl/4.5-mmol·L^{-1} KCl at the mucosal side (as indicated by the schematic inset). (b) Transient stimulation of a K^+-permeable apical conductance measured in the presence of 107-mmol·L^{-1} NMDG Cl/4.5-mmol·L^{-1} KCl at the mucosal side (as indicated by the schematic inset). Values are means (solid lines) ± SEM (dotted lines); n = 8 for both experimental series. Time-dependent controls (n = 8) show no changes in I_{sc}.

On average, the negative I_{sc} induced by BzATP amounted to −0.25 ± 0.09 μEq·h^{-1}·cm^{-2} (n = 8; $P < 0.05$ vs. baseline).

3.4 | Sensitivity of the BzATP response to antagonists of P2X receptors

Experiments with receptor antagonists were performed in order to functionally characterize the P2X receptors stimulated by BzATP ($5{\cdot}10^{-5}$ mol·L^{-1}). A438079 (10^{-4} mol·L^{-1} at the serosal side), a competitive P2X7 pore inhibitor (Haanes & Edvinsson, 2014), did not reduce the current induced by serosal BzATP (Table 2). In the presence of this inhibitor, however, the response evoked by the cAMP-dependent secretagogue forskolin, but not that induced by the Ca^{2+}-dependent secretagogue carbachol, was significantly reduced, which might suggest that either the action of forskolin possibly involves the stimulation of ATP release from cells in the mucosa or the submucosa or that the P2X7 antagonist nonspecifically interferes with cAMP signalling. In contrast, in the presence of AZ10606120 ($5{\cdot}10^{-5}$ mol·L^{-1} at the serosal side), a noncompetitive P2X7 antagonist, which acts as negative allosteric modulator (Haanes & Edvinsson, 2014), the current evoked by serosal BzATP was inhibited by >85% ($P < 0.05$; Figure 4a, b). BzATP also is known to stimulate P2X4 receptors, for example, in rat liver (Emmett et al., 2008). Therefore, the sensitivity of the I_{sc} response evoked by serosal BzATP to 5-BDBD, a P2X4 antagonist (Coddou et al., 2019), was tested. Indeed, 5-BDBD (10^{-5} mol·L^{-1} at the serosal side) significantly inhibited the current induced by serosal BzATP by about 70% (Table 2 and Figure 4c,d). When BzATP was administered at the mucosal side, AZ10606120 ($5{\cdot}10^{-5}$ mol·L^{-1} at the mucosal side) completely suppressed the I_{sc} evoked by the purinergic agonist, whereas mucosal 5-BDBD did not inhibit the BzATP-induced current significantly (Table 3).

3.5 | BzATP effects on cytosolic Ca^{2+} concentration

The tetrodoxin-resistant response to mucosal BzATP (Table 3) suggests the presence of ionotropic P2X receptors on the colonic epithelium. In order to prove this assumption, experiments with isolated colonic crypts loaded with the Ca^{2+}-sensitive fluorescent dye, fura-2, were performed. Indeed, BzATP ($5{\cdot}10^{-5}$ mol·L^{-1}) induced a prompt increase in the fura-2 fluorescence ratio indicating an increase in the cytosolic Ca^{2+} concentration (Figure 5). This has to be expected when P2X receptors, that is, ligand-gated nonselective cation channels, are activated and Ca^{2+} enters the cytosol. From 132 measured cells, 80% responded with an increase in the fura-2 ratio (for definition of responders, see Methods), which on average amounted to 0.73 ± 0.05 (n = 105). Administration of the SERCA inhibitor cyclopiazonic acid (CPA; $5{\cdot}10^{-6}$ mol·L^{-1}) as a viability control at the end of the experiments induced a prompt increase in the fura-2 ratio (Figure 5).

3.6 | Comparison with native ATP

The question arises whether native ATP, the physiological agonist for purinoceptors, also activates ionotropic P2X receptors in colonic mucosa. Therefore, concentration–response curves were performed with serosal or mucosal administration of ATP. As for BzATP, serosal ATP had a higher efficiency to induce an increase in I_{sc} in comparison

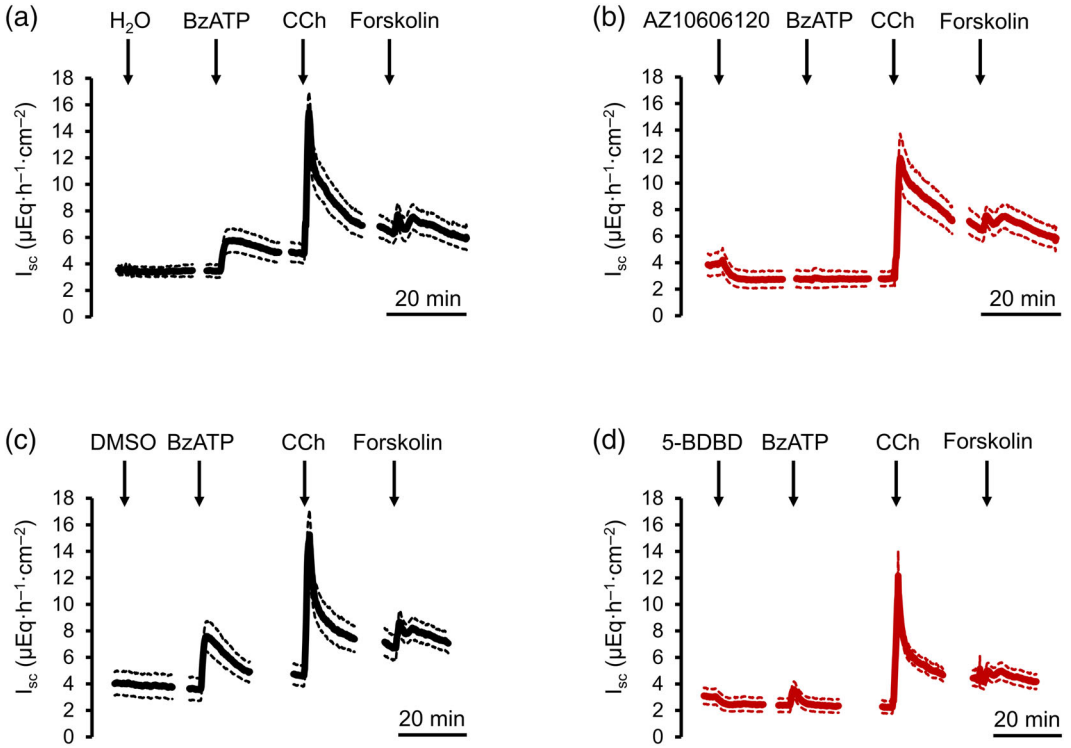

FIGURE 4 Effect of BzATP ($5{\cdot}10^{-5}$ mol·L^{-1} at the serosal side) on I_{sc} in the absence (a) or presence (b) of the P2X7 receptor blocker AZ10606120 ($5 \cdot 10^{-4}$ mol·L^{-1} at the serosal side) or in the absence (c) or presence (d) of the P2X4 receptor antagonist 5-BDBD (10^{-5}-mol·L^{-1} serosal). At the end of each experiment, carbachol (CCh; $5 \cdot 10^{-5}$-mol·L^{-1} serosal) and forskolin ($9 \cdot 10^{-6}$-mol·L^{-1} mucosal and serosal) were administered as viability controls. Control tissues were treated with the solvents for the individual receptor blockers (DMSO in case of 5-BDBD, water in the case of AZ10606120). Line interruptions are caused by omission of time intervals in order to synchronize the tracings of individual records to the administration of the next drug. Values are means (solid lines) ± SEM (dotted lines); n = 8 for all experimental series; for statistics, see Table 2.

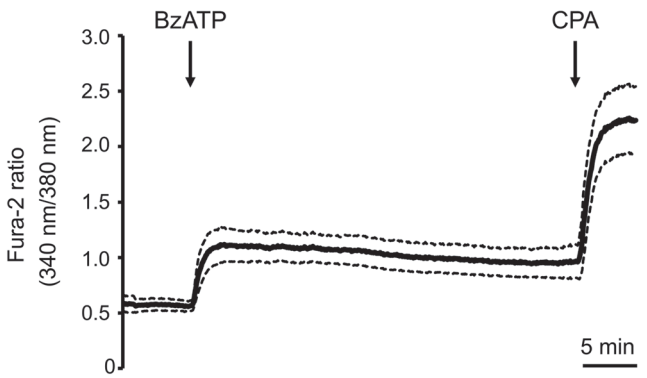

FIGURE 5 Effect of BzATP ($5{\cdot}10^{-5}$ mol·L^{-1}) on the fura-2 ratio signal of epithelial cells located in an isolated colonic crypt. At the end of the experiment, cyclopiazonic acid (CPA; $5{\cdot}10^{-6}$ mol·L^{-1}) was administered as viability control. Values are means (solid line) ± SEM (dotted lines); n = 12; for statistics, see text.

to mucosal ATP (Figure 6). In contrast to BzATP, ATP (10^{-4} mol·L^{-1}) induced a stronger increase in G_t after serosal administration (5.71 ± 0.83 mS·cm^{-2}, $P < 0.05$, n = 6) in comparison to mucosal administration (0.52 ± 0.14 mS·cm^{-2}, $P < 0.05$, n = 6). As initially observed by Cuthbert and Hickman (1985), the increase in I_{sc} induced by serosal ATP was inhibited by tetrodotoxin by about 65% ($P < 0.05$, n = 6, Figure 7 and Table 4), whereas—similar to BzATP—the current induced by mucosal ATP was not significantly affected by the tetrodotoxin (Table 5). Cholinergic neurotransmission seems to be involved in the stimulation of secretomotor submucosal neurons because hexamethonium (10^{-4} mol·L^{-1} at the serosal side) diminished the current induced by serosal ATP by 30% ($P < 0.05$, n = 6), although atropine was ineffective (Table 4). These results might indicate that predominantly non-cholinergic secretomotor neurons are activated by ATP. A putative candidate contributing to the communication between the secretomotor neurons and the epithelium may be vasoactive intestinal peptide (**VIP**), which beside **acetylcholine** is often the predominant prosecretory neurotransmitter found in the submucosal plexus of different species and different intestinal segments (Krueger et al., 2016). Another plausible candidate may be nitric oxide (**NO**), as it has been shown in rat colon that nearly all neurons expressing NO synthase are also immunoreactive for P2X7 (Girotti et al., 2013). As for BzATP, the effect of serosal ATP was significantly diminished by the P2X4 receptor blocker, 5-BDBD, as well as by the P2X7 receptor blocker, AZ10606120, with A438079 being ineffective (Table 4). In the case of mucosal ATP, only AZ10606120 numerically reduced the ATP-induced I_{sc} by about one third (without reaching statistical significance), whereas A438079 and 5-BDBD had no effect (Table 5).

Ivermectin is known to potentiate the actions of agonists at P2X4 receptors (see, e.g., Stokes & Surprenant, 2009). Consequently, it was tested in orientating experiments whether ivermectin in different concentrations (ranging from 3 to 50 · 10^{-6} mol·L^{-1} at the mucosal side) might be able to enhance the effect of mucosal ATP. However, the 'most efficient' combination of 10^{-5} mol·L^{-1} ivermectin with 10^{-4} mol·L^{-1} ATP only tended to enhance the effect of ATP (Table 5) suggesting that apical P2X4 receptors do not play a major role in the control of transepithelial ion transport.

As for BzATP (see above), we tested for the possible involvement of neuronal $P2Y_1$ receptors in the effect of serosal ATP. In the presence of the $P2Y_1$ antagonist MRS2500 (10^{-6} mol·L^{-1} at the serosal side), ATP (10^{-4} mol·L^{-1} at the serosal side) induced an increase in I_{sc} of 4.09 ± 0.39 μEq·h^{-1}·cm^{-2} (n = 6), which was significantly ($P < 0.05$) reduced to 2.45 ± 0.58 μEq·h^{-1}·cm^{-2} (n = 6), when the tissues also were pretreated with tetrodotoxin (10^{-6} mol·L^{-1} at the serosal side), indicating a prominent contribution of P2X receptors to the excitation of secretomotor neurons.

In order to exclude that ATP might have been converted to adenosine by ectoATPases in the apical membrane of the epithelium, it was tested whether the ectoATPase inhibitor, ARL67156 (10^{-4} mol·L^{-1} at the mucosal side), did reduce the I_{sc} evoked by mucosal ATP. However, this was not the case suggesting that cleavage products of ATP are not involved in the induction of electronic response of the epithelium (Table 5).

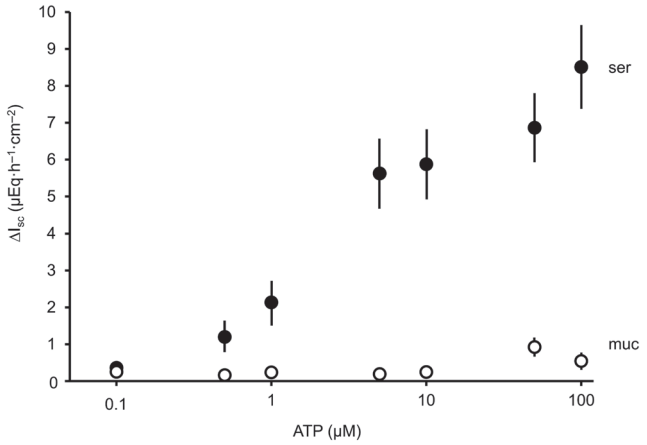

FIGURE 6 Concentration-dependent effect of adenosine triphosphate (ATP) on I_{sc} administered at the serosal (black circles) or mucosal (open circles) side of rat distal colon. After each administration, the compartment to which ATP had been applied was washed three times with 5× the chamber volume. The curves were constructed from two independent experimental series, in which concentrations from 10^{-7}–10^{-6} or 10^{-6}–10^{-4} mol·L^{-1}, respectively, were administered. Data are given as difference to the baseline I_{sc} just prior administration of ATP (ΔI_{sc}) and are means (symbols) ± SEM (lines; within the size of the symbols for mucosal ATP); n = 6 for each group (except for the concentration of 10^{-6} mol·L^{-1}, where the data from both experimental series were pooled, i.e., n = 12).

3.7 | Apical ion currents induced by native ATP

Besides the expected activation of a nonselective cation conductance after P2X receptor stimulation (Figure 3a), the experiments with basolaterally depolarized epithelia suggested the activation of a small K^+ current across the apical membrane (Figure 3b). In order to prove this with an obviously more efficient agonist, mucosal ATP was administered under the same ionic conditions as depicted in Figure 3b, that is, with 107 mmol·L^{-1} NMDGCl/4.5 mmol·L^{-1} KCl at the mucosal and 111.5 KCl mmol·L^{-1} at the serosal side. Under these conditions, native ATP (10^{-4} mol·L^{-1} at the mucosal side) also induced a transient negative I_{sc} which amounted to −0.64 ± 0.19 μEq·h^{-1}·cm^{-2} (n = 8; $P < 0.05$ vs. time-dependent control), whereas the current remained stable in time-dependent control experiments performed at the same time (n = 7).

3.8 | Expression of P2X receptors on mRNA level

In order to prove the expression of different P2X receptors (P2X1 - P2X7) in rat colon, RT-PCR experiments were performed. Because both tetrodotoxin-sensitive effects, that is, neuronally

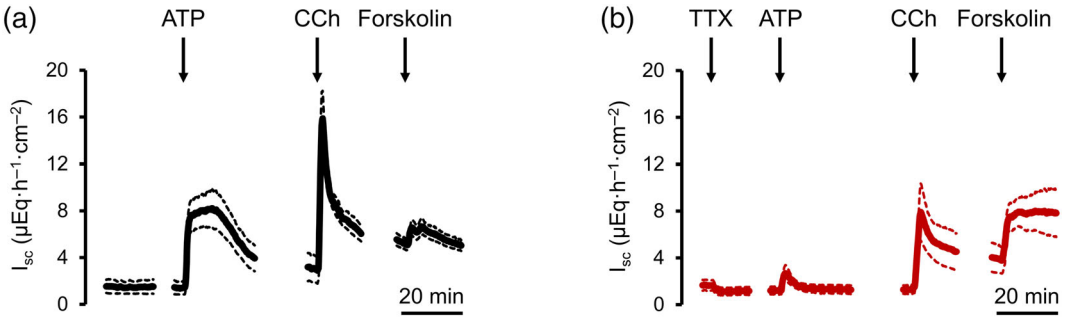

FIGURE 7 Effect of adenosine triphosphate (ATP) (10^{-4} mol·L^{-1} at the serosal side) on I_{sc} in the absence (a) or presence (b) of tetrodotoxin (TTX, 10^{-6} mol·L^{-1} at the serosal side). At the end of each experiment, carbachol (CCh; $5 \cdot 10^{-5}$ mol·L^{-1} serosal) and forskolin ($9 \cdot 10^{-6}$ mol·L^{-1} mucosal and serosal) were administered as viability controls. Line interruptions are caused by omission of time intervals in order to synchronize the tracings of individual records to the administration of the next drug. Values are means (solid lines) ± SEM (dotted lines); n = 6 for all experimental series; for statistics, see Table 4.

TABLE 4 Effect of ATP administered to the serosal side of distal colon

	Change in ATP response	ATP (10^{-4} mol·L^{-1})	Carbachol ($5{\cdot}10^{-5}$ mol·L^{-1})	Forskolin ($9{\cdot}10^{-6}$ mol·L^{-1})	n
			ΔI_{sc} (μEq·h^{-1}·cm^{-2})		
Serosal side					
– Tetrodotoxin		7.50 ± 1.20	14.85 ± 1.50	1.72 ± 0.32	6
+ Tetrodotoxin (10^{-6} mol·L^{-1})	↓	2.75 ± 0.67*	8.69 ± 2.49*	8.61 ± 1.40$^{P = 0.06}$	6
– Hexamethonium		7.68 ± 0.84	14.15 ± 1.20	3.49 ± 0.51	7
+ Hexamethonium (10^{-4} mol·L^{-1})	↓	5.34 ± 0.57*	14.15 ± 1.88	3.43 ± 0.71	6
– Atropine		8.02 ± 1.53	14.65 ± 1.40	3.93 ± 1.30	8
+ Atropine (10^{-6} mol·L^{-1})		7.33 ± 0.70	3.75 ± 0.73*	11.97 ± 0.74*	8
– A438079		6.29 ± 0.62	9.94 ± 1.28	3.32 ± 0.55	6
+ A438079 (10^{-4} mol·L^{-1})		5.90 ± 0.80	10.23 ± 1.07	2.36 ± 0.34	6
– AZ10606120		5.03 ± 0.84	11.21 ± 1.25	2.42 ± 0.54	7
+ AZ10606120 ($5{\cdot}10^{-5}$ mol·L^{-1})	↓	0.87 ± 0.21*	8.89 ± 1.52	3.32 ± 0.48	7
– 5-BDBD		6.18 ± 0.89	11.37 ± 1.16	2.43 ± 0.40	8
+ 5-BDBD (10^{-5} mol·L^{-1})	↓	2.84 ± 0.57*	12.52 ± 1.64	0.53 ± 0.16*	8

Note: Increase in I_{sc} induced by adenosine triphosphate (ATP) (at the serosal side), carbachol (at the serosal side) and forskolin (at the mucosal and serosal side) in rat distal colon. Responses were tested in the presence and absence of different drugs administered on the serosal side. A438079 and AZ10606120 are used as P2X7 antagonists, 5-BDBD as P2X4 antagonist. Effects of drugs on baseline I_{sc} are shown in Table S1 (pooled data from all experiments depicted in Tables 2–5 with the same inhibitor). Values are given as change in I_{sc} versus baseline just prior administration of the individual secretagogue (ΔI_{sc}) and are means ± SEM.
*P < 0.05 versus response of the same secretagogue in the corresponding control series.

TABLE 5 Effect of ATP administered to the mucosal side of distal colon

	Change in ATP response	ATP (10^{-4} mol·L^{-1})	Carbachol($5{\cdot}10^{-5}$ mol·L^{-1})	Forskolin ($9{\cdot}10^{-6}$ mol·L^{-1})	n
			ΔI_{sc} (μEq·h^{-1}·cm^{-2})		
Mucosal side					
– ARL67156		1.45 ± 0.17	12.10 ± 1.09	2.23 ± 0.25	6
+ ARL67156 (10^{-4} mol·L^{-1})		1.30 ± 0.31	13.52 ± 1.71	1.11 ± 0.40*	6
– A438079		1.64 ± 0.35	13.78 ± 0.35	1.68 ± 0.50	6
+ A438079 (10^{-4} mol·L^{-1})		1.55 ± 0.30	14.35 ± 1.52	2.05 ± 0.15	6
– AZ10606120		1.55 ± 0.25	11.97 ± 1.66	3.78 ± 0.54	7
+ AZ10606120 ($5{\cdot}10^{-5}$ mol·L^{-1})	(↓)	0.97 ± 0.16$^{P = 0.08}$	8.39 ± 1.81	3.53 ± 0.50	6
– 5-BDBD		0.81 ± 0.12	11.17 ± 1.47	1.93 ± 0.24	7
+ 5-BDBD (10^{-5} mol·L^{-1})		0.82 ± 0.29	11.55 ± 1.50	1.21 ± 0.23	7
– Ivermectin		1.15 ± 0.27	9.89 ± 2.12	1.17 ± 0.24	7
+ Ivermectin (10^{-5} mol·L^{-1})		1.92 ± 0.31	13.12 ± 1.37	1.58 ± 0.40	8
Serosal side					
– Tetrodotoxin		1.58 ± 0.42	13.15 ± 0.97	2.99 ± 0.71	6
+ Tetrodotoxin (10^{-6} mol·L^{-1})		0.66 ± 0.13	12.22 ± 2.52	2.77 ± 0.43	6

Note: Increase in I_{sc} induced by adenosine triphosphate (ATP) (at the mucosal side), carbachol (at the serosal side) and forskolin (at the mucosal and serosal side) in rat distal colon. Responses were tested in the presence and absence of different drugs administered on either the mucosal or serosal side. ARL67156 was used as ectoATPase blocker, A438079 and AZ10606120 as P2X7 antagonists, and 5-BDBD as P2X4 antagonist. Effects of drugs on baseline I_{sc} are shown in Table S1 (pooled data from all experiments depicted in Tables 2–5 with the same inhibitor). Values are given as change in I_{sc} versus baseline just prior administration of the individual secretagogue (ΔI_{sc}) and are means ± SEM.
*P < 0.05 versus response of the same secretagogue in the corresponding control series.

mediated responses, as well as putatively direct epithelial effects (e.g., evoked by mucosal administration of ATP or BzATP) had been observed, homogenates both from intact colonic wall (containing plexus of the enteric nervous system) as well as mucosal scrapings were used as starting material for mRNA isolation. Different tissues such as spinal cord, dorsal root ganglia, kidney or liver were used as positive controls. With the exception of P2X6, amplificates of the expected size (Table 1) of all P2X receptor subtypes were found in the colonic samples (Figures 8 and 9). P2X6 mRNA, however, was neither found in the colonic samples nor in the reference tissues used (Figure 8b). P2X7 receptors can be quite divergent with profound species differences (Donnelly-Roberts et al., 2009) and expression of different splice variants - albeit often with impaired function (Shokoples et al., 2021). However, one of these isoforms, P2X7(k), with an alternative exon 1, shows a higher sensitivity to BzATP in comparison to the full-length receptor P2X7(a) (Liang et al., 2019; Nicke et al., 2009). Amplificates for this isoform were detected in the colonic samples, too (Figure 9b). The efficiency of RNA isolation and cDNA synthesis was verified by using GAPDH-specific primers. The water control without template cDNA showed no amplificates (Figure 9). Sequencing of the PCR products revealed an identity of ≥97.3% with the corresponding target structures for all products.

3.9 | Immunohistochemical localization of P2X4 and P2X7 receptors

Immunohistochemical staining with primary antibodies directed against P2X4 or P2X7, respectively, was performed to investigate the expression and the localization within the colonic wall on the protein level for both receptors. Immunopositive signals for both receptors were found in the colonic epithelium with a predominant expression in the more mature epithelial cells at the surface and the upper third of the crypts (Figure 10). Immunoreactivity was found also in cells within the submucosa or between the longitudinal and the circular layer of the tunica muscularis. These cells also were immunopositive for the neuronal marker, MAP 2, indicating that they represent neurons of the submucosal and the myenteric plexus. Negative controls

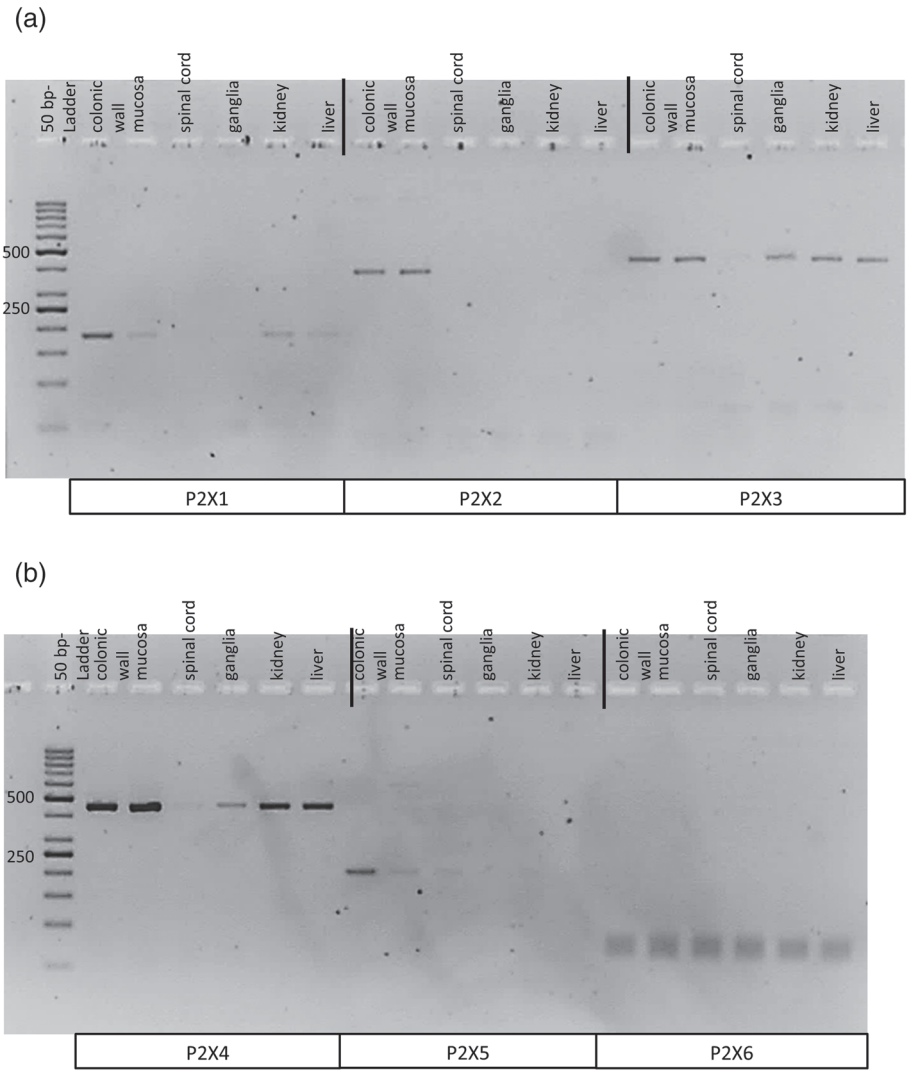

FIGURE 8 Reverse transcriptase polymerase chain reaction (RT-PCR) detection of mRNA expression of P2X1–P2X3 (a) or P2X4–P2X6 receptors (b) in samples from intact colonic wall or colonic mucosa. For expected size of the amplificates, see Table 1. The cDNA from spinal cord, dorsal root ganglia, kidney or liver was used as positive control. Shown are representative results from three independent experiments (three biological and two technical replicates).

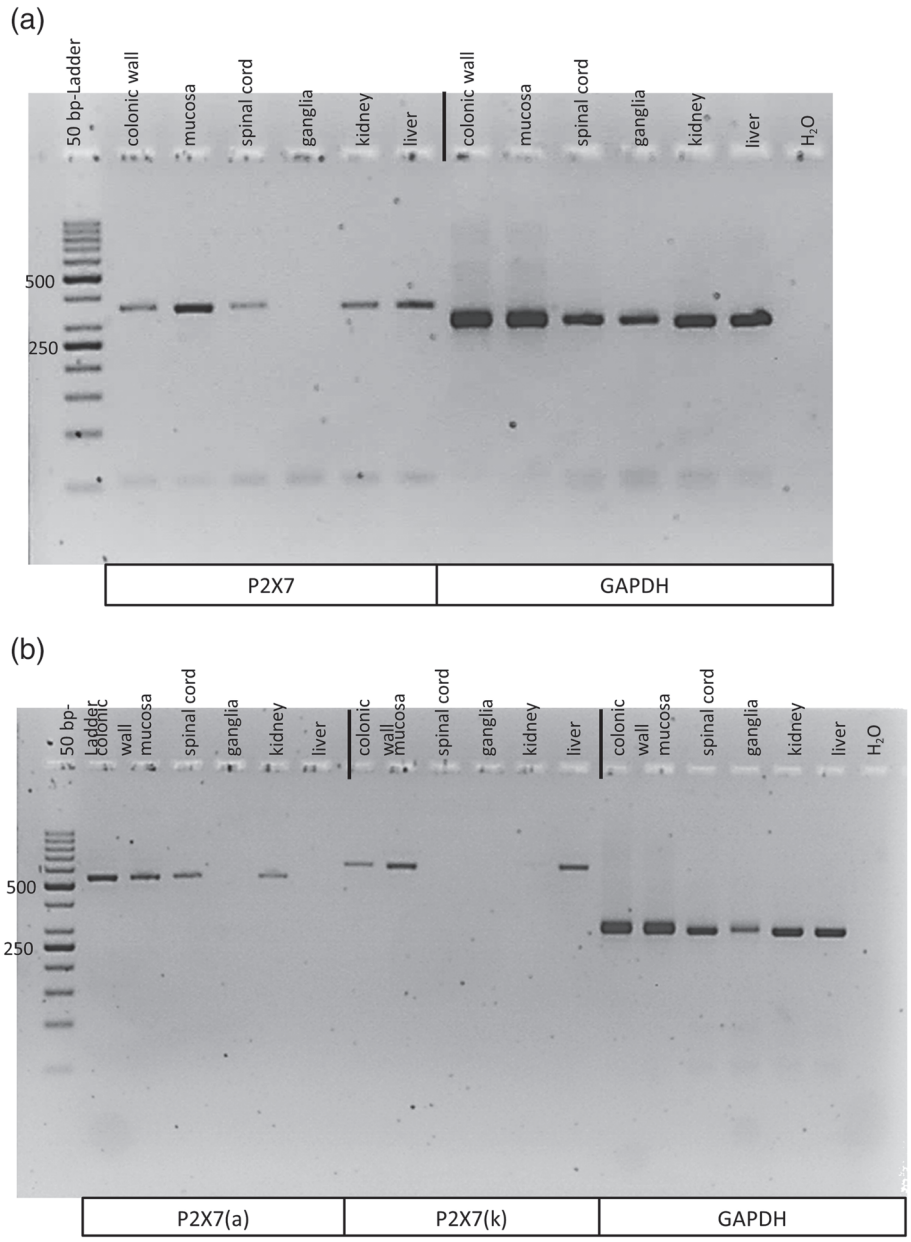

FIGURE 9 Reverse transcriptase polymerase chain reaction (RT-PCR) detection of mRNA expression of P2X7 (a) and the splice variant P2X7(k) in comparison to the full-length receptor (termed P2X7(a) here in analogy to the reference from Nicke et al., 2009; b) in samples from intact colonic wall or colonic mucosa. For expected size of the amplificates, see Table 1. The cDNA from spinal cord, dorsal root ganglia, kidney or liver was used as positive control. The efficiency of RNA isolation and cDNA synthesis was verified by using GAPDH-specific primers (303 bp). The water control without template cDNA showed no amplificates. Shown are representative results from three independent experiments (three biological and two technical replicates).

without the primary antibodies did not reveal in any signals (Figure 10).

Attempts to characterize the P2X receptors in the submucosal ganglia, which are found occasionally (depending on the cutting plane) in the immunostainings of the colonic sections (Figure 10), more systematically in whole-mount preparations failed, as obviously the antibodies, especially that used against P2X7, showed a strong nonspecific background binding in these thick preparations. However, the main aim of the present study was to clarify the question whether also in the intestine epithelial P2X receptors are involved in the regulation of ion transport (see Introduction) and both the expression of P2X4 and P2X7 in rat enteric neurons has already been well documented in the literature (Bo et al., 2003; Girotti et al., 2013). Thus, no further attempts were performed to characterize MAP 2-positive cells expressing P2X4 or P2X7 in more detail.

4 | DISCUSSION

4.1 | Expression and functional significance of ionotropic P2X in the colonic wall

The present results demonstrate that BzATP, a purine analogue known to act on P2X7 and in addition on P2X4 receptors (Emmett et al., 2008; Haanes et al., 2012), stimulates transepithelial currents across rat distal colon. The colon has a typical intestinal epithelium with the ability to switch between absorption and secretion in dependence on various neuronal, endocrine or paracrine signals. Functional experiments with tetrodotoxin, a neurotoxin, which suppresses the propagation of action potentials in neurons via blockade of voltage-dependent Na^+ channels (Catterall, 1980), indicate that secretomotor neurons within the submucosal plexus are the primary target of

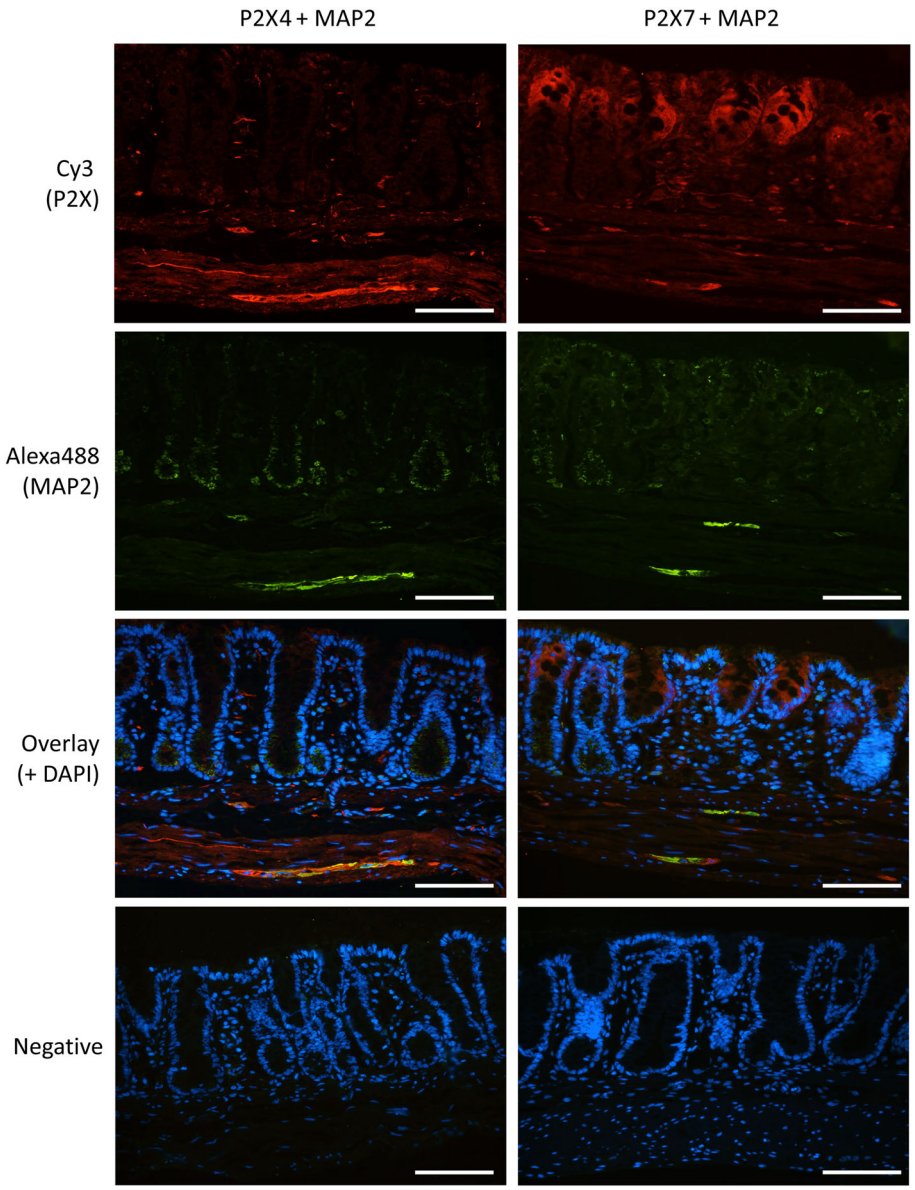

FIGURE 10 Immunofluorescent staining of rat distal colon with antibodies against P2X4 and P2X7 (red, coupled with Cy3) combined with the neuronal marker MAP 2 (green, coupled with Alexa488). The first row shows the red channel (Cy3), the second row the green channel (Alexa488) and the third row the overlay with DAPI, which was used for nucleus staining. Negative controls without the primary antibodies were performed in parallel (bottom). Scale bar is set to 100 μm. Representative staining from three independent experiments.

BzATP after serosal administration (Table 2), whereas mucosal BzATP seems to act directly at the epithelium, inducing a transepithelial current insensitive to tetrodotoxin (Table 3). Immunohistochemical labelling confirmed the expression of both P2X4 and P2X7 receptors in submucosal neurons as well as in the epithelium, especially in the surface region and the upper parts of the crypts (Figure 10). Consequently, these data show that purinergic control of intestinal ion transport is not solely mediated by metabotropic P2Y receptors, which were known for more than 20 years to play an important role in the regulation of epithelial transporters (Kerstan et al., 1998; Köttgen et al., 2003; Leipziger et al., 1997; Yamamoto & Suzuki, 2002), but also by ionotropic P2X receptors.

For native ATP, neuronal, that is, tetrodotoxin-sensitive effects after serosal administration (Figure 7 and Table 4) as well as tetrodotoxin-insensitive, presumably direct epithelial effects after mucosal administration (Table 5) were observed, too. The ectoATPase inhibitor ARL67156 did not reduce the I_{sc} evoked by mucosal ATP (Table 5). This finding is in contrast to the colonic tumour cell line, T84, where degradation of ATP to adenosine with subsequent stimulation of **A2 receptors** mediates the response to mucosal ATP (Stutts et al., 1995). Experiments with antagonists for P2X4 and P2X7 receptors confirm the involvement of both types of ionotropic receptors in the neuronally mediated responses evoked by serosal BzATP or ATP. Both were inhibited significantly by the P2X7 antagonist, AZ10606120, as well as by the P2X4 antagonist, 5-BDBD (Figure 4 and Tables 2 and 4), suggesting the functional significance of the two ionotropic receptor types for secretomotor neuron activation. The epithelial effect of mucosal BzATP, however, was suppressed only by the P2X7 antagonist, AZ10606120, but was not affected by 5-BDBD (Table 3). Similarly, the response to native ATP proved to be resistant against 5-BDBD, when the agonist was administered at the mucosal side, whereas AZ10606120 reduced the response numerically by about 35% (Table 5). The missing effect of 5-BDBD and the failure to enhance the response evoked by mucosal ATP with ivermectin, which

is known to potentiate the stimulation of murine P2X4 and also human (but not murine) P2X7 (Nörenberg et al., 2012), suggest that epithelial P2X4 receptors play no or only a very minor role in the control of colonic ion transport. The large AZ10606120-resistant response evoked by mucosal ATP is consistent with the well-known action of ATP on metabotropic $P2Y_2$ or $P2Y_6$ receptors expressed in the apical membrane of the colonic epithelial cells (Köttgen et al., 2003).

Surprisingly, another P2X7 antagonist, A438079, proved to be completely ineffective against the actions of the mucosally or serosally administered purinergic agonists (Tables 2–5). A similar pattern, that is, inhibition of the proliferation of pancreatic stellate cells by AZ10606120, but not by A438079, has already been observed by Haanes et al. (2012). The reasons may lay in the different modes of actions of both drugs. The competitive inhibitor A438079 seems to act primarily via prevention of pore formation, whereas the noncompetitive inhibitor AZ10606120 acts as negative allosteric modulator (Haanes et al., 2012).

A critical point in the pharmacological analyses of receptor functions is the specificity and the selectivity of the agonists used (recently reviewed by Illes et al., 2021). For example, BzATP, the prototypical P2X7 agonist (being here more potent than the native agonist, ATP), stimulates also **P2X1**, P2X2, **P2X3** and P2X4 receptors (Illes et al., 2021). Better is the situation for the antagonists. For example, the IC_{50} values of 5-BDBD (used as P2X4 receptor antagonist) are several times lower for P2X4 than for other P2X receptors, where this drug has been investigated. In the case of the two P2X7 receptors antagonists tested, A-438079 and AZ10606120, the affinity (based on IC_{50} values) of A-438079 is much higher for P2X7 than for the other six P2X receptors (Illes et al., 2021). Unfortunately, for AZ10606120, that is, the inhibitor which proved to be effective in the rat colon, no such comparisons are available yet (Illes et al., 2021). Thus, it cannot be excluded with certainty that inhibition of the response to serosal BzATP or mucosal BzATP by AZ10606120 (Tables 2 and 3) might be caused by nonselective inhibition of other purinergic receptors. However, as stated above, AZ10606120 is primarily a negative allosteric modulator and also in other biological systems such as pancreatic stellate cells discrepancies between competitive inhibition by A438079 and AZ10606120 have been observed (Haanes et al., 2012). The situation is further complicated by the fact that the trimeric P2X receptors do not only occur as homomers but can in addition form heteromers, which will probably strongly affect sensitivity against different receptor blockers. Even more, most data in the literature refer to human or mouse P2X receptors, but strong species differences are known, for example, in agonist-induced cation currents across P2X receptors (Jiang et al., 2013) or pharmacological properties such as the interaction of ivermectin, which potentiates the stimulation of human, but not rat P2X7 (Nörenberg et al., 2012).

P2X7 receptors are known to need a relatively high concentration of ATP to be activated and are more sensitive to BzATP than to native ATP (Sluyter, 2017). In the present experiments, when fitting the concentration response curves of serosal BzATP (Figure 1) and serosal ATP (Figure 6) to a Hill equation, the half-maximal concentration needed for BzATP was even higher (8 $\mu mol \cdot L^{-1}$) compared to ATP (2 $\mu mol \cdot L^{-1}$); thus, ATP seemed to be more effective. This discrepancy might be explained by the assumption that BzATP stimulates in addition other ionotropic receptors such as P2X4 as suggested by the inhibitor experiments (Tables 2–5).

4.2 | Ion transport mechanisms regulated by ionotropic P2X receptors

Different ionic mechanisms are obviously involved in the induction of transepithelial currents by serosal or mucosal BzATP. In the case of serosal administration with the simultaneous stimulation of secretomotor neurons within the enteric nervous system, the BzATP-induced I_{sc} reflects secretion of Cl^- as indicated by anion replacement experiments. This is consistent with the sensitivity against bumetanide, an inhibitor of the basolateral Na^+-K^+-$2Cl^-$-cotransporter acting as the dominant Cl^--loading transporter in the basolateral membrane (Table 2). As the BzATP-induced Cl^- secretion proved to be resistant against atropine, neuronal P2X4 and P2X7 receptors seem to be located on non-cholinergic secretomotor neurons. However, the observation that a biological response (such as Cl^- secretion) evoked by a purinergic agonist is sensitive to tetrodotoxin does not necessarily imply that the corresponding receptors stimulated by the agonist must be localized on neurons. Instead, a stimulation of other cell types (such as macrophages) releasing mediators finally stimulating the secretomotor neurons might be possible as well.

In contrast, the current induced by mucosal BzATP was independent from the presence of Cl^- and resistant to bumetanide indicating that ionic transport processes other than Cl^- secretion must be the underlying mechanism (Table 3). The most plausible explanation might be the assumption that the I_{sc} activated by mucosal BzATP is caused by an ion flux across apical ionotropic P2X receptors, which function as nonselective ligand-gated cation channels (Burnstock, 2018). Electrically, both the secretion of anions (such as Cl^-) as well as the electrogenic flux of cations (such as Na^+) from the mucosal to the serosal side of the tissue induce a positive I_{sc}. The stimulation of Na^+ flux across the apical membrane was proven in tissues which had been basolaterally depolarized in order to bypass the basolateral membrane. Under these conditions, BzATP induced a sustained positive I_{sc} (Figure 3a). This positive current was suppressed in the absence of Na^+ in the mucosal compartment. Thus, the I_{sc} induced by mucosal BzATP is carried by cation flux, either via P2X channels and/or via cation channels activated after P2X receptor stimulation (see below). Furthermore, under these conditions a small negative I_{sc} induced by BzATP, which would be in accordance with the transient activation of K^+ secretion, was uncovered (Figure 3b).

The currents induced by serosal as well as by mucosal BzATP were strongly inhibited by serosal Ba^{2+} (Tables 2 and 3). Ba^{2+}, which blocks most K^+ channels in the basolateral membrane, leads to a strong depolarization of the membrane (Böhme et al., 1991). Thereby, the driving force for both Cl^- secretion activated by serosal BzATP as

well as electrogenic Na^+ influx induced by mucosal BzATP will be reduced. At first glance, it seems surprising that mucosal Ba^{2+} also suppressed the electrogenic response evoked by BzATP administered to the same compartment (Table 3). The transient K^+ secretion induced by the purinergic agonist suggested by the experiments with basolaterally depolarized epithelia (Figure 3b) should induce a negative I_{sc} and thereby reduce the positive I_{sc} induced by an absorptive Na^+ flux. In other words, mucosal Ba^{2+} would be expected to enhance rather than to inhibit the current stimulated by mucosal BzATP (see Table 3). However, Ba^{2+} in the molar concentration range obviously inhibits the binding of BzATP on P2X7 receptors (Virginio et al., 1997), which might explain the unexpected observation.

Activation of the epithelial P2X receptors was concomitant with an increase in the cytosolic Ca^{2+} concentration, as shown by experiments at isolated colonic crypts loaded with the Ca^{2+}-sensitive fluorescent dye, fura-2 (Figure 5). These experiments do not allow to distinguish between the activation of P2X receptors in the apical membrane (underlying the response to mucosal BzATP in the Ussing chamber experiments) or in the basolateral membrane (responsible for the small, albeit directly measurable increase in I_{sc} evoked by serosal BzATP in the presence of tetrodotoxin; Table 2). However, these results are in accordance with the known Ca^{2+}-permeability of most P2X receptors (Ohta et al., 2005). An increase in the cytosolic Ca^{2+} concentration is well known to activate epithelial K^+ channels, also in the apical membrane (Schultheiss & Diener, 1997), which might underlie the transient negative current across the apical membrane suggested by the experiments with basolaterally depolarized epithelia (Figure 3b). Furthermore, the Ca^{2+} influx evoked by activation of P2X7 also might stimulate other ion channels such as **TRPM4** or **TRPM5**, which function as Ca^{2+}-activated Na^+ channels (Clapham et al., 2005) in intestinal epithelia (Murakami et al., 2003). Such a (speculative) mechanism would enhance the cation current induced by BzATP across the apical membrane measured in the basolateral depolarization experiments (Figure 3a).

For several P2X receptors such as homomeric P2X2, P2X4 and P2X7 as well as various heterometric subunit combinations, a so-called pore dilatation is known, allowing a flux even of larger cations such as, for example, $NMDG^+$ after prolonged receptor activation (Harkat et al., 2017). Such a delayed pore dilatation might be the reason for the slowly developing time course of the I_{sc} induced by mucosal BzATP, which was paralleled by an increase in G_t (Figure 2). However, as the effect of BzATP was completely reversible upon washout, this increase in tissue conductance was obviously not accompanied by cellular damage.

4.3 | Clinical aspects of P2X4 and P2X7 receptors

During inflammatory responses including inflammatory bowel diseases, both immune cells such as, for example, dendritic cells or macrophages (Dosch et al., 2018) as well as activated glial cells (Vieira et al., 2014, 2017) release ATP, which modulates gastrointestinal functions such as motility, epithelial ion transport or neurotransmission in the enteric nervous system. In line with this, blockade of purinergic receptors such as P2X7 ameliorates the symptoms of experimental inflammatory bowel disease (Evangelinellis et al., 2022). A similar situation is observed, for example, in the cardiovascular system, where P2X7 receptors are assumed to contribute to the association between hypertension and low-grade chronic inflammation (Shokoples et al., 2021). Furthermore, several non-synonymous single nucleotide polymorphisms of P2X7 receptors are known. Some of them have been associated with human diseases such as bipolar disorder and depression, pain sensitivity, osteoporosis or pulmonary tuberculosis (Jiang et al., 2013). However, in the gut, no association of these polymorphisms with, for example, inflammatory bowel disease has been detected (Haas et al., 2007). Thus, P2X7 receptors, which are shown in the present study to be expressed in the colonic epithelium, too (Figures 8–10), play a central role in a great spectrum of diseases. Consequently, inhibition of this ionotropic receptor may serve as approach for the treatment of inflammatory bowel diseases (Magalhães & Castelucci, 2021).

4.4 | Conclusions

Taken together, these results indicate that besides the well-known neuronal P2X receptors expressed by enteric neurons (Ohta et al., 2005; Valdez-Morales et al., 2011; Yu et al., 2010), glial cells (Schneider et al., 2021) or many immune cells within the gastrointestinal wall (Kolachala et al., 2008), colonic epithelial cells also express different P2X receptors including P2X4 and P2X7 functionally involved in the control of electrogenic ion transport. Thus, these ionotropic 'danger signal' receptors (Stokes & Surprenant, 2009), which are well known to be coupled to the activation of **NLRP3** (nuclear oligomerization domain like receptor family pyrin domain containing 3) inflammasome (Shokoples et al., 2021), cell death (Haanes et al., 2012) or neuropathic pain (Zhang et al., 2020), obviously also are involved in the regulation of intestinal ion transport at the level of the colonic epithelium and may contribute to the pathogenesis of inflammatory bowel diseases as ATP is released in the gut under inflammatory conditions (Brown et al., 2016; Vieira et al., 2017).

DECLARATION OF TRANSPARENCY AND SCIENTIFIC RIGOUR

This Declaration acknowledges that this paper adheres to the principles for transparent reporting and scientific rigour of preclinical research as stated in the *BJP* guidelines for Natural Products Research, Design and Analysis, Immunoblotting and Immunochemistry, and Animal Experimentation, and as recommended by funding agencies, publishers and other organizations engaged with supporting research. Open Access funding enabled and organized by Projekt DEAL.

ACKNOWLEDGEMENTS

The diligent technical assistance of Mrs. Brigitta Buss, Bärbel Schmidt and Alice Stockinger is a pleasure to acknowledge. Open Access funding enabled and organized by Projekt DEAL.

CONFLICT OF INTEREST

The authors declare no conflict of interest. This Declaration acknowledges that this paper adheres to the principles for transparent reporting and scientific rigour of preclinical research as stated in the *BJP* guidelines for **Design & Analysis**, and **Animal Experimentation**, and as recommended by funding agencies, publishers and other organizations engaged with supporting research.

AUTHOR CONTRIBUTION

JB, RC and KR performed experiments. MD and VG drafted the manuscript. All authors planned the experiments and approved the final version.

DATA AVAILABILITY STATEMENT

The data that support the findings of this study are available from the corresponding author upon reasonable request. Some data may not be made available because of privacy or ethical restrictions.

ORCID

Martin Diener https://orcid.org/0000-0003-2194-4636

REFERENCES

Alexander, S. P., Kelly, E., Mathie, A., Peters, J. A., Veale, E. L., Armstrong, J. F., Faccenda, E., Harding, S. D., Pawson, A. J., Southan, C., Davies, J. A., Aldrich, R. W., Attali, B., Baggetta, A. M., Becirovic, E., Biel, M., Bill, R. M., Catterall, W. A., Conner, A. C., … Zhu, M. (2021). The concise guide to PHARMACOLOGY 2021/22. *British Journal of Pharmacology*, *178*(S1), S1–S513.

Alexander, S. P. H., Roberts, R. E., Broughton, B. R. S., Sobey, C. G., George, C. H., Stanford, S. C., Cirino, G., Docherty, J. R., Giembycz, M. A., Hoyer, D., Insel, P. A., Izzo, A. A., Ji, Y., MacEwan, D. J., Mangum, J., Wonnacott, S., & Ahluwalia, A. (2018). Goals and practicalities of immunoblotting and immunohistochemistry: A guide for submission to the British Journal of pharmacology. *British Journal of Pharmacology*, *175*, 407–411. https://doi.org/10.1111/bph.14112

Apolloni, S., Amadio, S., Montilli, C., Volonté, C., & D'Ambrosi, N. (2013). Ablation of P2X7 receptor exacerbates gliosis and motoneuron death in the SOD1-G93A mouse model of amyotrophic lateral sclerosis. *Human Molecular Genetics*, *22*, 4102–4116. https://doi.org/10.1093/hmg/ddt259

Bo, X., Kim, M., Nori, S. L., Schoepfer, R., Burnstock, G., & North, R. A. (2003). Tissue distribution of $P2X_4$ receptors studied with an ectodomain antibody. *Cell and Tissue Research*, *313*, 159–165. https://doi.org/10.1007/s00441-003-0758-5

Böhme, M., Diener, M., & Rummel, W. (1991). Calcium- and cyclic-AMP-mediated secretory responses in isolated colonic crypts. *Pflügers Archiv - European Journal of Physiology*, *419*, 144–151. https://doi.org/10.1007/BF00373000

Brown, I. A. M., McClain, J. L., Watson, R. E., Patel, B. A., & Gulbransen, B. D. (2016). Enteric glia mediate neuron death in colitis through purinergic pathways that require connexin-43 and nitric oxide. *Cellular and Molecular Gastroenterology and Hepatology*, *2*, 77–91. https://doi.org/10.1016/j.jcmgh.2015.08.007

Burnstock, G. (2016). Purinergic signalling in the gut. In S. Brierley & M. Costa (Eds.), *The enteric nervous system* (pp. 91–112). Springer International Publishing. https://doi.org/10.1007/978-3-319-27592-5_10

Burnstock, G. (2018). Purine and purinergic receptors. *Brain and Neuroscience Advances*, *2*, 1–10.

Burnstock, G., & Wong, H. (1978). Comparison of the effects of UV light and purinergic nerve stimulation on the Guinea-pig taenia coli. *British Journal of Pharmacology*, *62*, 293–302. https://doi.org/10.1111/j.1476-5381.1978.tb08459.x

Catterall, W. A. (1980). Neurotoxins that act on voltage-sensitive sodium channels in excitable membranes. *Annual Review of Pharmacology and Toxicology*, *20*, 15–43. https://doi.org/10.1146/annurev.pa.20.040180.000311

Clapham, D. E., Julius, D., Montell, C., & Schultz, G. (2005). International union of pharmacology. XLIX. Nomenclature and structure-function relationships of transient receptor potential channels. *Pharmacological Reviews*, *57*, 427–450. https://doi.org/10.1124/pr.57.4.6

Coddou, C., Sandoval, R., Hevia, M. J., & Stojilkovic, S. S. (2019). Characterization of the antagonist actions of 5-BDBD at the rat P2X4 receptor. *Neuroscience Letters*, *690*, 219–224. https://doi.org/10.1016/j.neulet.2018.10.047

Curtis, M. J., Alexander, S., Cirino, G., Docherty, J. R., George, C. H., Giembycz, M. A., Hoyer, D., Insel, P. A., Izzo, A. A., Ji, Y., MacEwan, D. J., Sobey, C. G., Stanford, S. C., Teixeira, M. M., Wonnacott, S., & Ahluwalia, A. (2018). Experimental design and analysis and their reporting II: Updated and simplified guidance for authors and peer reviewers. *British Journal of Pharmacology*, *175*, 987–993. https://doi.org/10.1111/bph.14153

Cuthbert, A. W., & Hickman, M. E. (1985). Indirect effects of adenosine triphosphate on chloride secretion in mammalian colon. *The Journal of Membrane Biology*, *86*, 157–166. https://doi.org/10.1007/BF01870782

Del Castillo, J. R. (1987). The use of hyperosmolar, intracellular-like solutions for the isolation of epithelial cells from Guinea-pig small intestine. *Biochimica et Biophysica Acta*, *901*, 201–208.

Diener, M., Knobloch, S. F., Bridges, R. J., Keilmann, T., & Rummel, W. (1989). Cholinergic-mediated secretion in the rat colon: Neuronal and epithelial muscarinic responses. *European Journal of Pharmacology*, *168*, 219–229. https://doi.org/10.1016/0014-2999(89)90568-2

Donnelly-Roberts, D. L., Namovic, M. T., Han, P., & Jarvis, M. F. (2009). Mammalian P2X7 receptor pharmacology: Comparison of recombinant mouse, rat and human P2X7 receptors. *British Journal of Pharmacology*, *157*, 1203–1214. https://doi.org/10.1111/j.1476-5381.2009.00233.x

Dosch, M., Gerber, J., Jebbawi, F., & Beldi, G. (2018). Mechanisms of ATP release by inflammatory cells. *International Journal of Molecular Sciences*, *19*, 1222. https://doi.org/10.3390/ijms19041222

Emmett, D. S., Feranchak, A., Kilic, G., Puljak, L., Miller, B., Dolovcak, S., McWilliams, R., Doctor, R. B., & Fitz, J. G. (2008). Characterization of ionotrophic purinergic receptors in hepatocytes. *Hepatology*, *47*, 698–705.

Evangelinellis, M. M., Souza, R. F., Mendes, C. E., & Castelucci, P. (2022). Effects of a P2X7 receptor antagonist on myenteric neurons in the distal colon of an experimental rat model of ulcerative colitis. *Histochemistry and Cell Biology*, *157*, 65–81. https://doi.org/10.1007/s00418-021-02039-z

Fuchs, W., Larsen, E. H., & Lindemann, B. (1977). Current-voltage curve of sodium channels and concentration dependence of sodium permeability in frog skin. *The Journal of Physiology*, *267*, 137–166. https://doi.org/10.1113/jphysiol.1977.sp011805

Girotti, P. A., Misawa, R., Palombit, K., Mendes, C. E., Bittencourt, J. C., & Castelucci, P. (2013). Differential effects of undernourishment on the differentiation and maturation of rat enteric neurons. *Cell and Tissue Research*, *353*, 367–380. https://doi.org/10.1007/s00441-013-1620-z

Haanes, K. A., & Edvinsson, L. (2014). Expression and characterization of purinergic receptors in rat middle meningeal artery – Potential role in migraine. *PLoS ONE*, *9*, e108782. https://doi.org/10.1371/journal.pone.0108782

Haanes, K. A., Schwab, A., & Novak, I. (2012). The P2X7 receptor supports both life and death in fibrogenic pancreatic stellate cells. *PLoS ONE*, *7*, e51164. https://doi.org/10.1371/journal.pone.0051164

Haas, S. L., Ruether, A., Singer, M. V., Schreiber, S., & Böcker, U. (2007). Functional P2X7 receptor polymorphisms (His155Tyr, Arg307Gln, Glu496Ala) in patients with Crohn's disease. *Scandinavian Journal of Immunology*, *65*, 166–170. https://doi.org/10.1111/j.1365-3083.2006.01876.x

Harding, S. D., Sharman, J. L., Faccenda, E., Southan, C., Pawson, A. J., Ireland, S., Gray, A. J. G., Bruce, L., Alexander, S. P. H., Anderton, S., Bryant, C., Davenport, A. P., Doerig, C., Fabbro, D., Levi-Schaffer, F., Spedding, M., Davies, J. A., & NC-IUPHAR. (2018). The IUPHAR/BPS guide to PHARMACOLOGY in 2018: Updates and expansion to encompass the new guide to IMMUNOPHARMACOLOGY. *Nucleic Acids Research*, *46*, D1091–D1106. https://doi.org/10.1093/nar/gkx1121

Harkat, M., Peverini, L., Cerdan, A. H., Dunning, K., Beudez, J., Martz, A., Calimet, N., Specht, A., Cecchini, M., Chataigneau, T., & Grutter, T. (2017). On the permeation of large organic cations through the pore of ATP-gated P2X receptors. *Proceedings of the National Academy of Sciences of the United States of America*, *114*, E3786–E3795. https://doi.org/10.1073/pnas.1701379114

Hodges, R. R., Vrouvlianis, J., Shatos, M. A., & Dartt, D. A. (2009). Characterization of $P2X_7$ purinergic receptors and their function in rat lacrimal gland. *Investigative Ophthalmology & Visual Science*, *50*, 5681–5689. https://doi.org/10.1167/iovs.09-3670

Hu, H. Z., Gao, N., Zhu, M. X., Liu, S., Ren, J., Gao, C., Xia, Y., & Wood, J. D. (2003). Slow excitatory synaptic transmission mediated by $P2Y_1$ receptors in the Guinea-pig enteric nervous system. *The Journal of Physiology*, *550*, 493–504. https://doi.org/10.1113/jphysiol.2003.041731

Illes, P., Müller, C. E., Jacobson, K. A., Grutter, T., Nicke, A., Fountain, S. J., Kennedy, C., Schmalzing, G., Jarvis, M. F., Stojilkovic, S. S., King, B. F., & Di Virgilio, F. (2021). Update of P2X receptor properties and their pharmacology: IUPHAR review 30. *Brit J Pharmacol*, *178*, 489–514. https://doi.org/10.1111/bph.15299

Jiang, L. H., Baldwin, J. M., Roger, S., & Baldwin, S. A. (2013). Insights into the molecular mechanisms underlying mammalian P2X7 receptor functions and contributions in diseases, revealed by structural modeling and single nucleotide polymorphisms. *Frontiers in Pharmacology*, *4*, Art. 55.

Keating, N., Dev, K., Hynes, A. C., & Quinlan, L. R. (2019). Mechanism of luminal ATP activated chloride secretion in a polarized epithelium. *The Journal of Physiological Sciences*, *69*, 85–95. https://doi.org/10.1007/s12576-018-0623-7

Kerstan, D., Gordjani, N., Nitschke, R., Greger, R., & Leipziger, J. (1998). Luminal ATP induces K^+ secretion via a $P2Y_2$ receptor in rat distal colonic mucosa. *Pflügers Archiv - European Journal of Physiology*, *436*, 712–716. https://doi.org/10.1007/s004240050693

Kolachala, V. L., Bajaj, R., Chalasani, M., & Sitaraman, S. V. (2008). Purinergic receptors in gastrointestinal inflammation. *American Journal of Physiology. Gastrointestinal and Liver Physiology*, *294*, G401–G410. https://doi.org/10.1152/ajpgi.00454.2007

Köttgen, M., Löffler, T., Jacobi, C., Nitschke, R., Pavenstädt, H., Schreiber, R., Frische, R., Nielsen, S., & Leipziger, J. (2003). P2Y6 receptor mediates colonic NaCl secretion via differential activation of cAMP-mediated transport. *The Journal of Clinical Investigation*, *111*, 371–379. https://doi.org/10.1172/JCI200316711

Krueger, D., Michel, K., Zeller, F., Demir, I. E., Ceyhan, G. O., Slotta-Huspenina, J., & Schemann, M. (2016). Neural influences on human intestinal epithelium in vitro. *The Journal of Physiology*, *594*, 357–372. https://doi.org/10.1113/JP271493

Leipziger, J., Kerstan, D., Nitschke, R., & Greger, R. (1997). ATP increases $[Ca^{2+}]_i$ and ion secretion via a basolateral P2Y receptor in rat distal colonic mucosa. *Pflügers Archiv - European Journal of Physiology*, *434*, 77–83.

Li, L. Z., Yue, L. H., Zhang, Z. M., Zhao, J., Ren, L. M., Wang, H. J., & Li, L. (2020). Comparison of mRNA expression of P2X receptor subtypes in different arterial tissues of rats. *Biochemical Genetics*, *58*, 677–690. https://doi.org/10.1007/s10528-020-09968-9

Liang, X., Samways, D. S. K., Cox, J., & Egan, T. M. (2019). Ca^{2+} flux through splice variants of the ATP-gated ionotropic receptor P2X7 is regulated by its cytoplasmic N terminus. *The Journal of Biological Chemistry*, *294*, 12521–12533. https://doi.org/10.1074/jbc.RA119.009666

Lilley, E., Stanford, S. C., Kendall, D. E., Alexander, S. P. H., Cirino, G., Docherty, J. R., George, C. H., Insel, P. A., Izzo, A. A., Ji, Y., Panettieri, R. A., Sobey, C. G., Stefanska, B., Stephens, G., Teixeira, M., & Ahluwalia, A. (2020). ARRIVE 2.0 and the British Journal of Pharmacology: Updated guidance for 2020. *British Journal of Pharmacology*, *177*, 3611–3616. https://doi.org/10.1111/bph.15178

Magalhães, H. I. R., & Castelucci, P. (2021). Enteric nervous system and inflammatory bowel diseases: Correlated impacts and therapeutic approaches through the P2X7 receptor. *World Journal of Gastroenterology*, *27*, 7909–7924. https://doi.org/10.3748/wjg.v27.i46.7909

Murakami, M., Xu, F., Miyoshi, I., Sato, E., Ono, K., & Iijima, T. (2003). Identification and characterization of the murine TRPM4 channel. *Biochemical and Biophysical Research Communications*, *307*, 522–528. https://doi.org/10.1016/S0006-291X(03)01186-0

Nicke, A., Kuan, Y. H., Masin, M., Rettinger, J., Marquez-Klaka, B., Bender, O., Górecki, D. C., Murrell-Lagnado, R. D., & Soto, F. (2009). A functional P2X7 splice variant with an alternative transmembrane domain 1 escapes gene inactivation in P2X7 knock-out mice. *The Journal of Biological Chemistry*, *284*, 25813–25822. https://doi.org/10.1074/jbc.M109.033134

Nörenberg, W., Sobottka, H., Hempel, C., Plötz, T., Fischer, W., Schmalzing, G., & Schaefer, M. (2012). Positive allosteric modulation by ivermectin of human but not murine P2X7 receptors. *British Journal of Pharmacology*, *167*, 48–66. https://doi.org/10.1111/j.1476-5381.2012.01987.x

Ohta, T., Kubota, A., Murakami, M., Otsuguro, K., & Ito, S. (2005). $P2X_2$ receptors are essential for $[Ca^{2+}]_i$ increases in response to ATP in cultured rat myenteric neurons. *American Journal of Physiology. Gastrointestinal and Liver Physiology*, *289*, G935–G948. https://doi.org/10.1152/ajpgi.00017.2005

Palombit, K., Mendes, C. E., Tavares-de-Lima, W., Barreto-Chaves, M. L., & Castelucci, P. (2019). Blockage of the P2X7 receptor attenuates harmful changes produced by ischemia and reperfusion in the myenteric plexus. *Digestive Diseases and Sciences*, *64*, 1815–1829. https://doi.org/10.1007/s10620-019-05496-8

Percie du Sert, N., Hurst, V., Ahluwalia, A., Alam, S., Avey, M. T., Baker, M., Browne, W. J., Clark, A., Cuthill, I. C., Dirnagl, U., Emerson, M., Garner, P., Holgate, S. T., Howells, D. W., Karp, N. A., Lazic, S. E., Lidster, K., MacCallum, C. J., Macleod, M., … Würbel, H. (2020). The ARRIVE guidelines 2.0: Updated guidelines for reporting animal research. *British Journal of Pharmacology*, *177*, 3617–3624. https://doi.org/10.1111/bph.15193

Pouokam, E., Bader, S., Brück, B., Schmidt, B., & Diener, M. (2013). ATP-sensitive K^+ channels in rat colonic epithelium. *Pflügers Archiv - European Journal of Physiology*, *465*, 865–877. https://doi.org/10.1007/s00424-012-1207-7

Schneider, R., Leven, P., Glowka, T., Kuzmanov, I., Lysson, M., Schneiker, B., Miesen, A., Baqi, Y., Spanier, C., Grants, I., Mazzotta, E., Villalobos-Hernandez, E., Kalff, J. C., Müller, C. E., Christofi, F. L., & Wehner, S. (2021). A novel P2X2-dependent purinergic mechanism of enteric gliosis in intestinal inflammation. *EMBO Molecular Medicine*, *13*, e12724.

Schultheiss, G., & Diener, M. (1997). Regulation of apical and basolateral K^+ conductances in the rat colon. *British Journal of Pharmacology*, *122*, 87–94. https://doi.org/10.1038/sj.bjp.0701353

Shokoples, B. G., Paradis, P., & Schiffrin, E. L. (2021). P2X7 receptors. An untapped target for the management of cardiovascular disease. *Arteriosclerosis, Thrombosis, and Vascular Biology*, *41*, 186–199. https://doi.org/10.1161/ATVBAHA.120.315116

Sim, J. A., Chaumont, S., Jo, J., Ulmann, L., Young, M. T., Cho, K., Buell, G., North, R. A., & Rassendren, F. (2006). Altered hippocampal synaptic potentiation in $P2X_4$ knock-out mice. *The Journal of Neuroscience*, *6*, 9006–9009.

Sluyter, R. (2017). The P2X7 receptor. *Advances in Experimental Medicine and Biology*, *1051*, 17–53. https://doi.org/10.1007/5584_2017_59

Stokes, L., & Surprenant, A. (2009). Dynamic regulation of the P2X4 receptor in alveolar macrophages by phagocytosis and classical activation. *European Journal of Immunology*, *39*, 986–995. https://doi.org/10.1002/eji.200838818

Stutts, M. J., Lazaruwski, E. R., Paradiso, A. M., & Boucher, R. C. (1995). Activation of CFTR cl^- conductance in polarized T84 cells by luminal extracellular ATP. *The American Journal of Physiology*, *268*, C425–C433. https://doi.org/10.1152/ajpcell.1995.268.2.C425

Valdez-Morales, E., Guerrero-Alba, R., Liñán-Rico, A., Espinosa-Luna, R., Zarazua-Guzman, S., Miranda-Morales, M., Montaño, L. M., & Barajas-López, C. (2011). P2X7 receptors contribute to the currents induced by ATP in Guinea pig intestinal myenteric neurons. *European Journal of Pharmacology*, *668*, 366–372. https://doi.org/10.1016/j.ejphar.2011.07.019

Vieira, C., Ferreirinha, F., Magalhães-Cardoso, M. T., Silva, I., Marques, P., & Correia-de-Sá, P. (2017). Post-inflammatory ileitis induces non-neuronal purinergic signaling adjustments of cholinergic neurotransmission in the myenteric plexus. *Frontiers in Pharmacology*, *8*, Art. 811.

Vieira, C., Magalhães-Cardoso, M. T., Ferreirinha, F., Silva, I., Dias, A. S., Pelletier, J., Sévigny, J., & Correia-de-Sá, P. (2014). Feed-forward inhibition of CD73 and upregulation of adenosine deaminase contribute to the loss of adenosine neuromodulation in postinflammatory ileitis. *Mediators of Inflammation*, 254640.

Virginio, C., Church, D., North, R. A., & Surprenant, A. (1997). Effects of divalent cations, protons and calmidazolium at the rat $P2X_7$ receptor. *Neuropharmacology*, *36*, 1285–1294. https://doi.org/10.1016/S0028-3908(97)00141-X

Yamamoto, T., & Suzuki, Y. (2002). Role of luminal ATP in regulating electrogenic $Na+$ absorption in Guinea pig distal colon. *American Journal of Physiology. Gastrointestinal and Liver Physiology*, *283*, G300–G308. https://doi.org/10.1152/ajpgi.00541.2001

Yu, Q., Zhao, Z. Q., Sun, J. H., Guo, W., Fu, J., Burnstock, G., He, C., & Xiang, Z. (2010). Expression of $P2X_6$ receptors in the enteric nervous system of the rat gastrointestinal tract. *Histochemistry and Cell Biology*, *133*, 177–188. https://doi.org/10.1007/s00418-009-0659-0

Zhang, W. J., Zhu, Z. M., & Liu, Z. X. (2020). The role and pharmacological properties of the P2X7 receptor in neuropathic pain. *Brain Research Bulletin*, *155*, 19–28. https://doi.org/10.1016/j.brainresbull.2019.11.006

SUPPORTING INFORMATION

Additional supporting information can be found online in the Supporting Information section at the end of this article.

How to cite this article: Ballout, J., Claßen, R., Richter, K., Grau, V., & Diener, M. (2022). Ionotropic P2X4 and P2X7 receptors in the regulation of ion transport across rat colon. *British Journal of Pharmacology*, 1–20. https://doi.org/10.1111/bph.15928